nature plants

Article

https://doi.org/10.1038/s41477-024-01698-9

Proxiome assembly of the plant nuclear pore reveals an essential hub for gene expression regulation

Received: 30 November 2023

Accepted: 11 April 2024

Published online: 21 May 2024

Check for updates

Yu Tang[1,2], Xiangyun Yang[2], Aobo Huang[3], Kyungyong Seong[1], Mao Ye[2], Mengting Li[3], Qiao Zhao[3], Ksenia Krasileva[1] & Yangnan Gu[1]

The nuclear pore complex (NPC) is vital for nucleocytoplasmic communication. Recent evidence emphasizes its extensive association with proteins of diverse functions, suggesting roles beyond cargo transport. Yet, our understanding of NPC's composition and functionality at this extended level remains limited. Here, through proximity-labelling proteomics, we uncover both local and global NPC-associated proteome in *Arabidopsis*, comprising over 500 unique proteins, predominantly associated with NPC's peripheral extension structures. Compositional analysis of these proteins revealed that the NPC concentrates chromatin remodellers, transcriptional regulators and mRNA processing machineries in the nucleoplasmic region while recruiting translation regulatory machinery on the cytoplasmic side, achieving a remarkable orchestration of the genetic information flow by coupling RNA transcription, maturation, transport and translation regulation. Further biochemical and structural modelling analyses reveal that extensive interactions with nucleoporins, along with phase separation mediated by substantial intrinsically disordered proteins, may drive the formation of the unexpectedly large nuclear pore proteome assembly.

The eukaryotic cell possesses a distinct subcellular compartment known as the nucleus, which is enclosed by a double-layered lipid membrane known as the nuclear envelope (NE)[1]. Spanning the NE are specialized molecular structures named nuclear pore complexes (NPCs), which play an essential role in mediating selective nucleocytoplasmic transport of macromolecules[2]. Assembled by sophisticated arrangement of ~500 to 1,000 nucleoporin proteins (Nups), the NPC architecture can be partitioned into the core scaffold and peripheral extensions[3]. The core scaffold is shaped by an 8-fold rotationally symmetrical Nup assembly, creating the NPC central channel—an essential conduit for the bidirectional transport of macromolecules[4]. The conduit is filled with intrinsically disordered Nups that contain phenylalanine–glycine (FG) repeats. These Nups are characterized by highly flexible FG-rich domains, which are separated by spacers of varying lengths[5] and interact with each other to establish the central channel barrier, enabling highly selective passage of nuclear transport receptors (NTRs) that carry cargos[6,7]. On the other hand, the asymmetric NPC peripheral extensions, including cytoplasmic filaments (CFs) and the nuclear basket (NB), form elongated, flexible filamentous structures that connect the NPC core with its immediate subcellular environment[2,8]. Specifically, at the NPC cytoplasmic surface, CFs emerge from the core scaffold and extend towards the cytoplasm[9]. Conversely, within the nucleus, the NB is composed of eight protein filaments originating from the NPC core scaffold or the NE and converging into a distal ring within the nuclear interior[10,11].

While the core scaffold of the NPC is highly conserved, the peripheral extensions of the NPC display notable structural plasticity and variations in composition among different eukaryotic species[12]. It is also noteworthy that these extensions have been reported to participate in regulating many biological processes independent of cargo transport.

[1]Department of Plant and Microbial Biology, University of California, Berkeley, CA, USA. [2]Institute of Advanced Agricultural Sciences, Peking University, Weifang, Shandong, China. [3]Center for Plant Biology, School of Life Sciences, Tsinghua University, Beijing, China. e-mail: guyangnan@berkeley.edu

Notable examples include the CF Nup, Nup358 and Nup214, which have been shown to interact with viral components and regulate the efficiency of viral replication and spread in human cells[13–15]. In addition, the FG-repeat motifs present in yeast CF Nups are involved in the positioning and remodelling of messenger ribonucleoprotein particles (mRNPs), thereby potentially influencing downstream translation processes[16]. At the inner nuclear periphery, the NB serves as the entry point for mRNA export and also plays a critical role in chromatin organization and transcription regulation[17]. For instance, the NB scaffold protein Mlp in yeasts and its homologue TPR in humans have been shown to form an extended filamentous network that selectively excludes the underlying heterochromatin and tethers actively transcribed chromatin within it[18,19]. In a recent pioneering study conducted in yeast, it was shown that Nup60, which harbours an array of short linear motifs, acts as a flexible suspension cable to anchor the NB to the nuclear pore membrane. This configuration also enables the structural flexibility of the NB in response to bulky cargo and changes in gene expression[20]. Interestingly, plants do not encode Nup358 and Nup60 orthologues. Instead, they have evolved specific Nups uniquely tailored for their own NPC extensions. For instance, the plant-specific Nup82 collaborates with Nup136 at the NB and functions in the activation of salicylic acid-mediated pathogen resistance in *Arabidopsis*[21]. In addition, another plant-specific NB nucleoporin, GBPL3, was recently identified as a functional bridge between the NB and the nucleoskeleton, thereby facilitating stress-related transcription regulation at the nuclear pore[22].

Advanced analytical techniques in comparative genomics, proteomics, cryo-electron microscopy and super-resolution microscopy have collectively elucidated the composition, organization and architecture of the NPC core scaffold with striking details in most taxa. However, the structure of NPC peripheral extensions remains largely uncharacterized[23–27]. Emerging evidence supports that the NPC is associated with a diverse array of proteins and protein complexes, thus encompassing a wide range of functions beyond cargo transport; nonetheless, our knowledge of the nuclear pore protein composition and function at this extended level are still restricted, especially in plants. Here, utilizing a modular-guided proximity-labelling proteomics approach, we report the assembly of the extended nuclear pore-associated proteome in *Arabidopsis*. Comprising more than 500 distinct proteins, this proteome is primarily linked to the peripheral extensions of the NPC and substantially expands the repertoire of NPC-associated proteins. A breakthrough from this research is a deeper molecular understanding of the NPC's role as an integrated platform for managing the flow of genetic information. The NPC achieves this by locally concentrating various molecular machineries for chromatin remodelling, transcriptional regulation and mRNA processing at the nuclear basket while simultaneously recruiting proteins regulating mRNA stability and translation to cytoplasmic filaments. These findings indicate that the NPC operates as a highly integrated platform to coordinate multiple steps of gene expression regulation.

Profile nuclear pore-associated proteome using proximity labelling

To gain a more complete understanding of the plant nuclear pore, particularly nuclear pore-associated proteins that extend beyond the well-characterized Nups, we aimed to identify proteins associated with the NPC extension structures. To achieve this goal, we selected two *Arabidopsis* nucleoporins, Nup50a from the NB and CG1 from the cytoplasmic filaments, as baits for proximity labelling (PL)-based proteomic profiling (Fig. 1a). Because both Nups contain FG repeats that potentially contribute to the selective cargo transport through the NPC, we fused the proximity-labelling enzyme to the distal end of their FG repeats to minimize potential labelling of cargo proteins (Extended Data Fig. 1a). We transformed the constructs into wild-type *Arabidopsis* and generated stable transgenic plants. Ten-day-old transgenic seedlings were used to perform proximity labelling, followed by total protein extraction, affinity purification of biotinylated protein and quantitative mass spectrometry as previously described[28,29]. Mock-treated transgenic plants (Mock) and biotin-treated wild-type non-transformants (NT) were included as control for the selection of specifically labelled protein candidates, and we used at least two biological replicates for each sample.

Spliceosomes are recruited to the NPC basket

Nup50 is a highly conserved FG-repeat nucleoporin that localizes to the NB in humans[30]. Consistently, in our previous PL proteomics profiling, we observed significant enrichment of Nup50a probed by other NB nucleoporins such as Nup82, GBPL3 and KAKU4, but it was not detected by non-NB nucleoporins (Extended Data Fig. 1b), supporting its specific localization at the NPC basket under native conditions in *Arabidopsis*. Using Nup50a as the bait for PL proteomics, we identified a total of 33 significantly enriched proteins (fold-change > 2, $P < 0.1$, peptide spectrum matches (PSM) > 1) (Fig. 1b and Supplementary Table 1). Among these candidates, we found the four most abundant and ubiquitously expressed importin-α proteins (IMPAs). This result is consistent with a previous IP–MS experiment using Nup50a-GFP[31] and offers additional evidence for the pertinent hypothesis that the disassembly of importin-α–cargo complexes and/or the assembly of importin-α–CAS is predominantly coordinated by the NPC basket[32]. Interestingly, in addition to IMPAs, we also found significant enrichment of spliceosome components ($P = 9.6 \times 10^{-05}$) and transcription regulators ($P = 4.9 \times 10^{-03}$) in the Nup50a proxiome (Fig. 1b right panel), suggesting that the NB may also engage in mRNA synthesis and processing.

To obtain a comprehensive understanding of proteins associated with the NPC basket, we combined the Nup50a proxiome with our previously collected PL proteomic datasets utilizing three other NB nucleoporin baits, including Nup82 (Extended Data Fig. 1c) (PXD015919), GBPL3 (ref. 22) (PXD032906) and KAKU4 (ref. 33) (PXD026924). This integration allowed us to reconstruct a comprehensive NB proxiome, which included 423 significantly enriched

Fig. 1 | Assembly of the nuclear basket proteome in *Arabidopsis* using PL proteomics. a, Schematic diagram depicting the NPC and Nups used as baits for PL proteomics in *Arabidopsis*. PL proteomic datasets obtained in this study are labelled in red, and those published previously are labelled in orange. ONM/INM, outer/inner nuclear membrane. **b**, Left: scatterplot displaying proteins identified in the Nup50a proxiome. Wild-type non-transformants treated with biotin (NT) and mock-treated *Nup50a-BioID2* transgenic plants (Mock) were used as controls for ratiometric analysis. Three biological replicates were used for each sample. Significantly enriched protein candidates were selected on the basis of cut-off $P < 0.1$ (two-sided *t*-tests without adjustment), fold-change > 2 and PSM > 1. Right: GO analysis of significantly enriched candidates, including importin-α proteins, spliceosome proteins and transcription regulatory proteins, with a heat map showing normalized PSM values of each prey. Underlying data can be found in Supplementary Table 1. **c**, Left: GO analysis of proxiomes identified by four different NB Nups. The four NB bait proteins are highlighted with blue octagons, while the shared GO terms of their preys are marked by red squares. A Venn diagram in the middle reveals 63 overlapping protein candidates identified by at least two NB Nups. Right: PPI networks within the integrated NB proxiome. In the PPI network among the 63 preys, blue and grey edges represent proximal associations identified in this study and experimentally determined interactions from the STRING database (https://string-db.org/), respectively. **d**, Top: comparative analysis of the NB proxiome and spliceosome proxiome defined by MAC3b. Bottom: GO analyses of NB-specific proteins and overlaps between NB proteins and spliceosome RNPs. **e**, Schematic model illustrating the association of the NB with various perinuclear proteins and protein complexes identified by PL, including the nucleoskeleton, importin-alphas and molecular machineries involved in gene expression regulation and subsequent mRNA splicing. Statistical test used for GO analysis in **b**–**d** was one-sided Fisher's exact test with multiple comparison adjustment.

https://doi.org/10.1038/s41477-024-01698-9

proteins (Fig. 1c and Supplementary Table 2). We then performed Gene Ontology (GO) analysis on the four individual proxiomes (Fig. 1c left panel) as well as on the integrated NB proteome (Extended Data Fig. 1d), which revealed an interesting functional network. As expected, the nucleoskeleton and the NPC core scaffold were found to be significantly enriched, consistent with the fact that these two structures are located in close proximity to the NB. Notably, the four separate proxiomes as well as the integrated NB proxiome all showed significant enrichment in spliceosome (Fig. 1c), indicating its robust association with the NPC basket.

Using 63 proteins that were probed by at least two NB baits, we constructed a protein–protein interaction (PPI) network using the Search Tool for the Retrieval of Interacting Genes/Proteins (STRING), which relies on previously published PPI data. This network reveals a wealth of interactions within the spliceosomal proteins that were identified (Fig. 1c right panel), implying that the NB probed not individual components but rather the entire spliceosomal complex as a whole. To substantiate this point, we compared spliceosome components identified in the NB proxiome with ribonucleoprotein (RNP) complexes probed by MAC3b[34], a core component of the Prp19 complex involved in splicing. The analysis revealed 171 overlaps between the two datasets, representing nearly half of MAC3b-identified RNPs (Fig. 1d). These 171 proteins encompassed all major RNA–protein subunits of the U1, U2, U4/U6 and

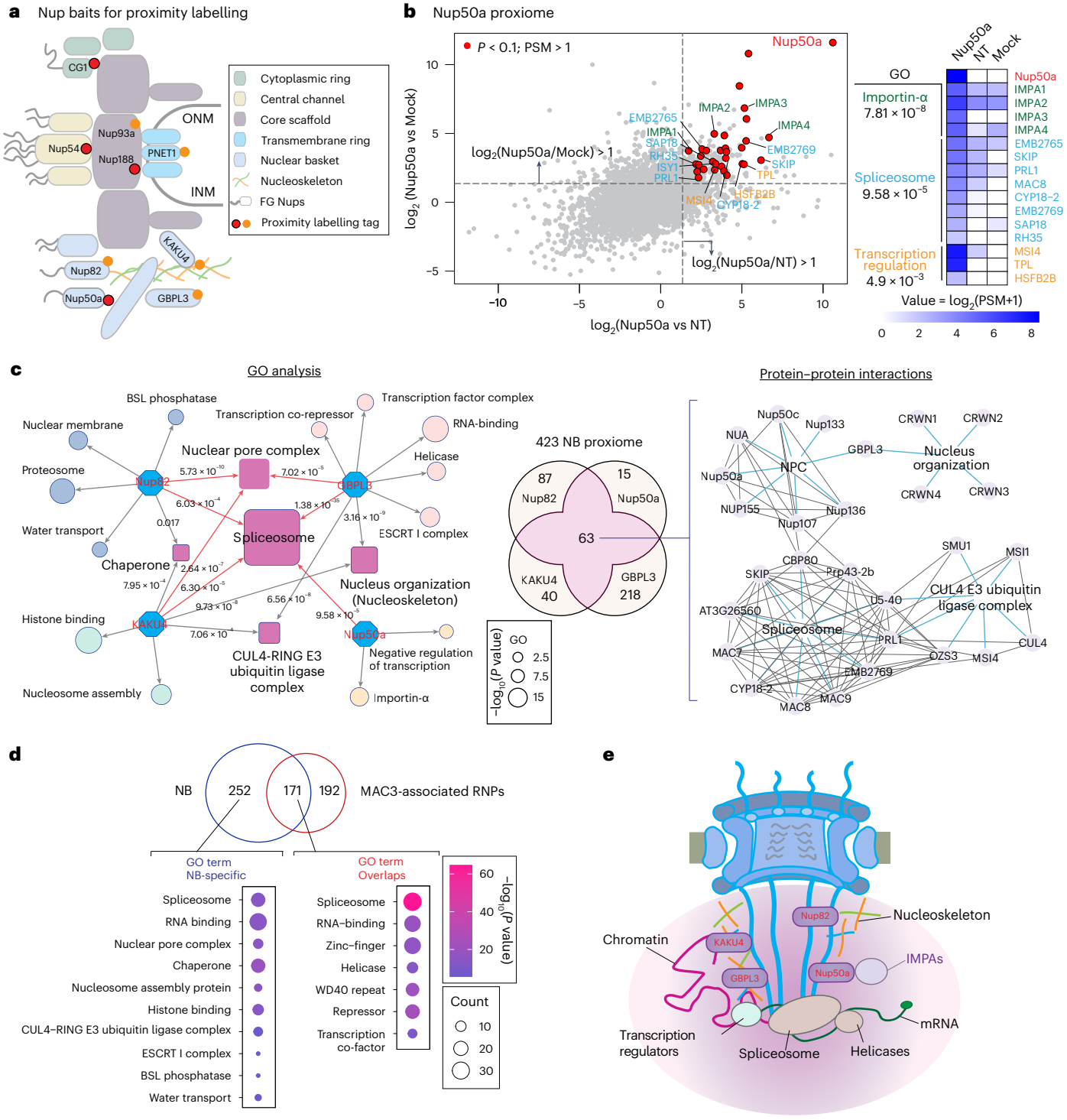

https://doi.org/10.1038/s41477-024-01698-9

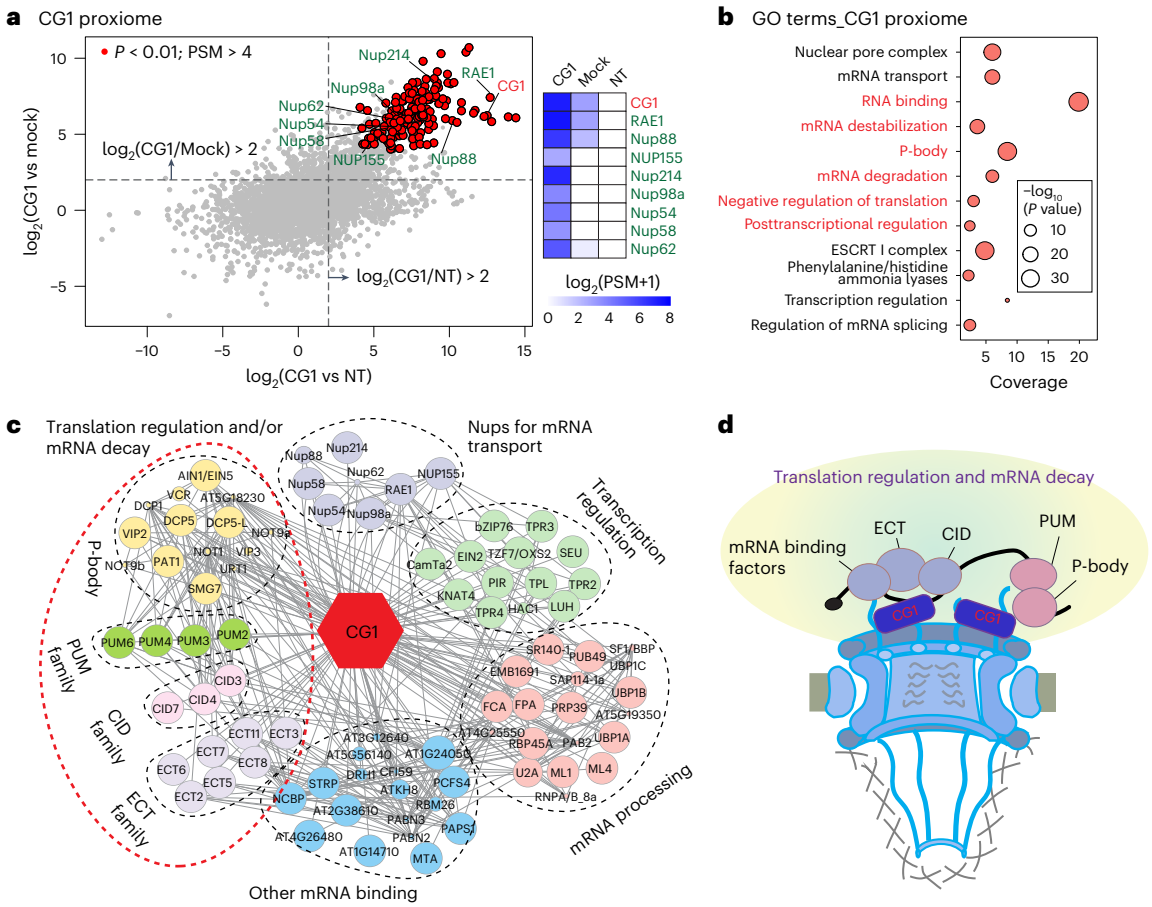

Fig. 2 | Recruitment of proteins involved in translation regulation to the cytoplasmic side of the nuclear pore. a, Left: scatterplot showing proteins identified in the CG1 proxiome. Known NPC components identified by CG1 are labelled. Controls for ratiometric analysis were mock-treated and non-transformant samples. Each sample had two biological replicates. Significantly enriched proteins, selected with cut-off $P < 0.01$ (two-sided *t*-test without adjustment), fold-change > 4 and PSM > 4, are denoted by red dots. Right: a heat map of PSM for known NPC components. Underlying data can be found in Supplementary Table 4. **b**, GO enrichment analysis of the CG1 proxiome. Molecular functions associated with translation regulation and mRNA decay are labelled in red. **c**, Functional subcategorization of 86 CG1 proximal proteins involved in transcription and translation regulation. Proteins were manually clustered and colour coded on the basis of their published functions. **d**, Schematic model illustrating the association of the NPC cytoplasmic filaments with proteins and protein complexes involved in regulating translation and mRNA stability. Statistical test used for GO analysis in **b** was a one-sided Fisher's exact test with multiple comparison adjustment.

U5 RNPs within the spliceosome. In addition, the NB proxiome also contains other spliceosome components and RNA-binding proteins that were not probed by MAC3b (Fig. 1d and Supplementary Table 3). These findings provide compelling evidence for the hypothesis that the NPC basket is associated with the spliceosome complex and its regulatory proteins (Fig. 1e).

It is worth noting that in addition to the spliceosome, the four NB baits display distinct protein associations (Fig. 1c). Specifically, the Nup50a proxiome exhibited a notable enrichment of importin-α proteins. Meanwhile, GBPL3 primarily identified transcription regulators and RNA-binding proteins. Nup82 displayed specific interactions with nuclear membrane proteins and proteasome components. Lastly, KAKU4 is located in a region populated by histone binding proteins and nucleosome assembly proteins, suggesting potential anchoring points for NPC–chromatin interactions. Because the four NB baits do not exhibit clear tissue- or cell-type-specific expression (Extended Data Fig. 1e), the profiling results suggest potential compositional complexity within the NB, which may serve as a multifaceted molecular platform capable of recruiting a diverse array of proteins. This recruitment, in turn, may support various nuclear processes at the NPC, including cargo transport, chromatin tethering, transcriptional regulation and protein degradation (Fig. 1e).

NPC cytoplasmic ring is enriched in translation regulators

To investigate potential proteins associated with the cytoplasmic facet of the NPC, we utilized a conserved cytoplasmic filament nucleoporin CG1 as bait for proximity labelling. Analysis of the CG1 proxiome identified 166 significantly enriched candidates (fold-change > 4, $P < 0.01$, PSM > 4), including four nucleoporins known to localize at the NPC cytoplasmic ring (RAE1, Nup88, Nup214 and Nup98a) and three central channel FG nucleoporins (Nup54, Nup58 and Nup62), ranked as top candidates (Fig. 2a and Supplementary Table 4). This result confirms that CG1 predominantly accumulates at the cytoplasmic side of the NPC in plant cells and suggests that this FG Nup may also be partially integrated into the Nup54/58/62 selective barrier network.

In addition to known NPC components, GO analysis of the CG1 proxiome revealed significant enrichment in proteins involved in mRNA-related function (Fig. 2b), which account for more than half (86/166) of the total CG1 proxiome. We subsequently constructed a PPI network among the 86 candidates using the STRING database, which further classified them into eight functional groups with five primary molecular functions, including mRNA decay, mRNA transport, transcription regulation, mRNA processing and other mRNA binding (Fig. 2c). Notably, half of these functional groups

are essential components of the P-body, pumilio (PUM) family proteins, CTC-interacting domain (CID) proteins and m^{6}A-containing RNA-binding protein evolutionary conserved C-terminal regions (ECTs). These proteins are known to play crucial roles in regulating mRNA translation, degradation and/or storage in cytoplasmic foci[35–39]. This finding indicates that mRNA molecules are probably subjected to translation-related regulation near the NPC cytoplasmic filaments, such as sequestration within P-bodies to prevent their translation or degradation, immediately after they are transported out of the nucleus (Fig. 2d). This result is also in line with previous animal studies suggesting that P granules are tethered to nuclear pores in the adult germline and the hypothesis that newly transcribed mRNAs are exported through P granule-associated NPCs[40].

We are surprised to find that some transcription regulators and spliceosome components are also present in the CG1 proxiome, although they are not significantly enriched in the GO analysis. Some of these overlapping candidates were identified by the NB nucleoporin GBPL3 (Extended Data Fig. 2). One possibility is that CG1 is a highly dynamic FG Nup and has multiple localizations within the NPC, including minor distribution at the inner face of the nuclear periphery[31,41]. Alternatively, some of the mRNA binding proteins may be transported together with mature mRNA to the cytoplasmic side of the NPC or co-translated with CG1 during NPC assembly[42]. Nonetheless, it is evident that the GBPL3 and CG1 proxiomes exhibit distinct protein compositions. The GBPL3 proxiome predominantly encompasses proteins associated with transcription regulation and nascent mRNA processing, while the CG1 proxiome is primarily centred on translation and RNA stability regulation (Extended Data Fig. 2 bottom). This underscores the difference in protein recruitment between the nucleoplasmic and cytoplasmic sides of the NPC.

NPC is an integrated platform for gene expression regulation

In addition to the nuclear basket and cytoplasmic filaments, we also performed PL-based proteomic profiling using the central channel barrier nucleoporin Nup54 and the core scaffold nucleoporin Nup188 (Extended Data Figs. 3a,b, and Supplementary Tables 5 and 6). Proteins probed by Nup54 and Nup188 further expand the proxiome of the NPC core scaffold that was previously defined by PL proteomics using Nup93a and PNET1 as bait (Extended Data Fig. 3c). For example, we identified three 14-3-3 proteins (GRF2/3/4) belonging to a family of conserved phospho-binding proteins that regulate several vital cellular processes by interacting with various binding partners[43,44]. In addition, Nup188 probed several other interesting factors, including chaperones and proteasome components, such as BIP1, CPN21 and UBP13 (Extended Data Fig. 3c). These proteins were also probed by NB proxiome, providing further evidence of their association with the NPC.

To obtain a comprehensive NPC-associated proteome, we integrated the Nup50a, CG1, Nup54 and Nup188 data with five previously obtained PL proteomics datasets (Nup93a, Nup82, GBPL3, PNET1 and KAKU4 from PXD015919, PXD026924 and PXD032906). The combined NPC-associated proteome contains 32 out of the 39 nucleoporins identified in *Arabidopsis*, with a majority of them being repeatedly probed by different Nup baits (Fig. 3a), indicating a thorough and extensive coverage. However, we missed four nucleoporins from the NPC outer ring complex (ORC), probably because we did not include ORC nucleoporins as bait in our profiling. This absence reinforces the stringent labelling radius of the PL enzyme, effectively confining the probed protein population to the immediate vicinity of the NPC. Notably, we also did not identify three membrane-associated nucleoporins: ALADIN, CPR5 and NDC1. We speculate that these nucleoporins may be expressed at a level beyond our detection limit or in a tissue- or cell-type-specific manner. Alternatively, these proteins may be embedded within the NPC in a way that precludes efficient labelling.

Compared with the well-characterized NPC composition, the NPC-associated proteome was significantly expanded and comprised 582 unique proteins (Fig. 3b and Supplementary Table 7). On the basis of their published or predicted molecular functions, we categorized 410 of these proteins into functional complexes or subgroups. The analysis revealed a predominant association of chromatin remodellers and transcription regulators with the nuclear basket, including proteins involved in chromatin remodelling, DNA binding, histone binding and modification, nucleosome assembly, Mediator and SAGA complexes, transcription factors and other transcription regulators, providing compelling evidence for the active involvement of the plant NPC in the regulation of gene expression. Moreover, regulators of mRNA processing are primarily enriched at the nuclear basket region, with 11 relevant functional subgroups identified. These subgroups function in various steps of RNA processing, including pre-mRNA biogenesis, mRNA splicing and disassembly of spliceosome after splicing is completed (Fig. 3b and Supplementary Table 8). These results suggest that the plant NPC basket is a platform that integrates transcription regulation with active pre-mRNA splicing, which presumably facilitates rapid transcriptional responses.

In contrast to the NPC basket, we found that regulators of mRNA translation are enriched on the cytoplasmic side of the NPC, which can be clustered into 5 functional subgroups. These subgroups include eukaryotic elongation factors for translation elongation, GYF proteins involved in mRNA metabolism, and P-body, ECT and PUM family proteins that participate in translation repression and/or mRNA destabilization (Fig. 3b). This finding indicates that the mRNA buffering may occur at the cytoplasmic side of the NPC, potentially preventing excessive translation or degradation of mRNA immediately after they are exported to the cytoplasmic side of the NPC.

NPC-associated proteins interact broadly with nucleoporins

Previously, we demonstrated a robust transcriptional correlation among *Arabidopsis* nucleoporin genes[12]. Here we expanded the investigation to include the newly discovered NPC-associated components, particularly those involved in transcription regulation, pre-mRNA splicing and translation regulation. Remarkably, upon examining the expression of these genes using available RNA-seq data, we found that over two-thirds of the NPC-associated genes exhibit strong co-expression with nucleoporin genes (Fig. 3c and Supplementary Table 9). In contrast, when we randomly selected genes from the *Arabidopsis* genome, we did not observe a comparable co-expression pattern. The coordinated gene expression supports functional connections between the identified NPC-associated proteins with the NPC core.

Fig. 3 | Assembly of the NPC-associated proteome in *Arabidopsis*. a, Heat map of normalized average PSM values for 32 nucleoporins (horizontal label) obtained through PL proteomics using 9 nucleoporins as baits (vertical label). Red and blue dots represent $P < 0.01$ and <0.05 (two-sided *t*-tests without adjustment), respectively, compared to controls. Nucleoporins are horizontally arranged on the basis of their location in different NPC modules. **b**, Integrated networks of proteins identified by 9 nucleoporin baits (hexagons outlined in red) using PL proteomics. Nucleoporins (represented as hexagons) and the proteins they probed (represented as circles) were placed in proximity to the NPC structure, corresponding to their potential locations as determined by the bait Nups that probed them. These proteins were grouped into three main categories: transcription regulation, mRNA splicing and processing, and translation regulation. Subcategories were manually clustered and colour coded on the basis of their established or predicted protein functions. **c**, Heat map illustrating the co-expression patterns of nucleoporin genes with other NPC-associated components identified in this study, particularly the three major functional categories shown in **b**. Co-expression among nucleoporins serves as the positive control, while random genes selected from the *Arabidopsis* genomes are used as the negative control. Greater edge weight corresponds to stronger co-expression.

https://doi.org/10.1038/s41477-024-01698-9

To validate the physical interactions between the newly identified NPC-associated proteins and nucleoporins, we conducted co-immunoprecipitation (co-IP) assays and confirmed in vivo associations between selected candidates and the NPC (Fig. 4a). However, co-IP validation was limited to a relatively small scale. In pursuit of a more comprehensive understanding of the molecular

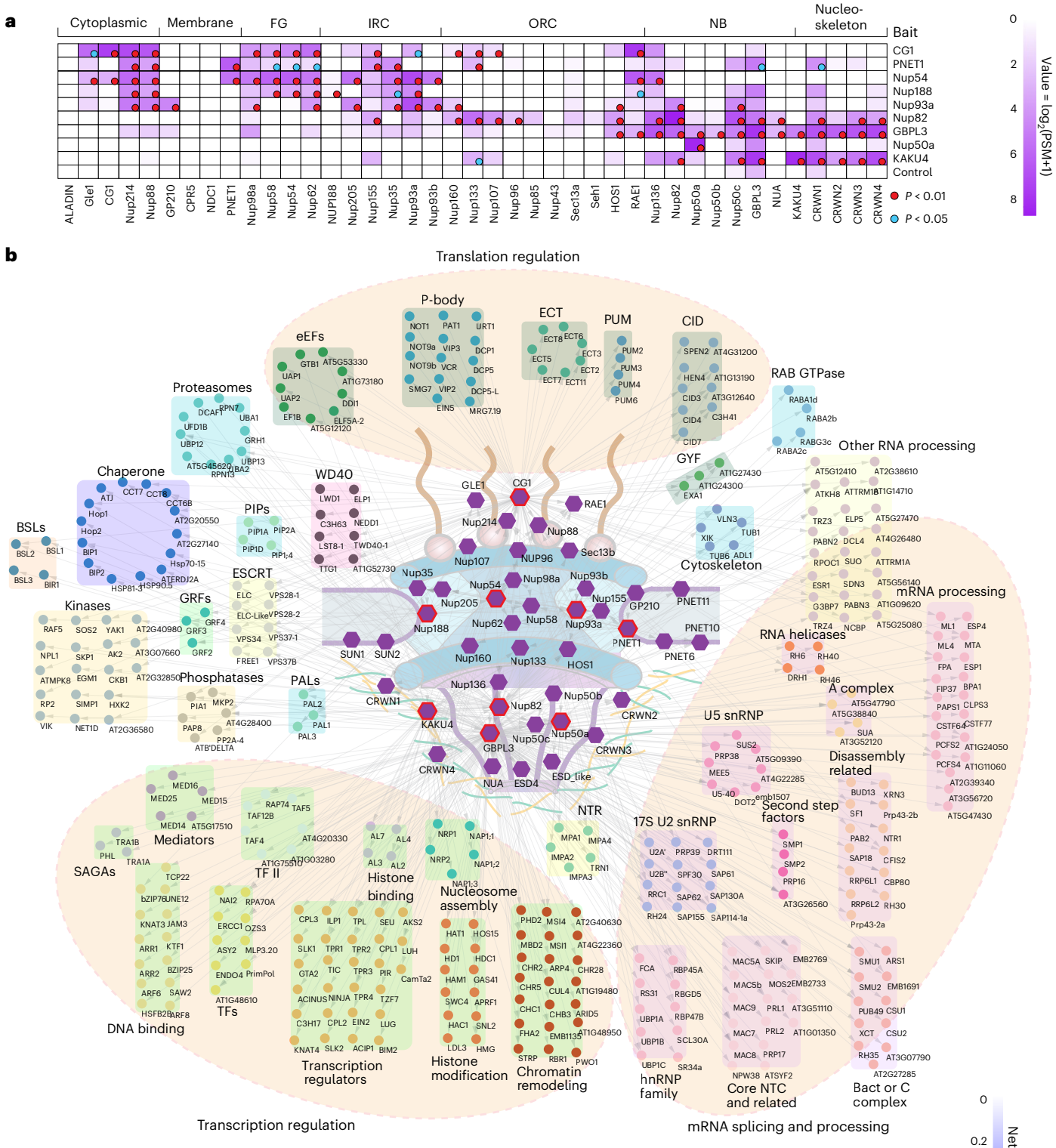

mechanisms underlying protein assembly around the NPC, we harnessed AlphaFold-Multimer for structural modelling and PPI prediction. Due to computational limitations, the combined amino acid (aa) length of the two predicted interacting partners was limited to 2,500 aa. Therefore, heterodimer complexes were predicted only for 109 NPC-associated proteins and nucleoporins whose combinations comply with this limitation. With the 109 proteins, we modelled 5,474 heterodimer complexes, which comprise more than 90% of all possible pairwise interactions (Extended Data Fig. 4a and Supplementary Table 10).

To filter for reliable interaction models, we used the intrinsic model accuracy estimate values iptm > 0.75 and pTM > 0.3 (for AlphaFold-Multimer) and the interface score > 0.5 (for AF2Complex) as cut-offs, resulting in 81 high-confidence PPI models (Fig. 4b, accessible through Zenodo at https://doi.org/10.5281/zenodo.10023066 (ref. 45)). Despite inherent limitations in the in silico PPI prediction, we obtained a remarkable validation rate. Specifically, about half of the high-confidence Nup–Nup interactions predicted (17 out of 37) were supported by electron microscopy-based structural analyses of the human NPC (Fig. 4c top panel). This result not only reinforces the reliability of the predicted PPIs but also suggests that these nucleoporin interactions are conserved between human and plant systems. We also found potential new interactions between plant-specific nucleoporins within or between different NPC modules, including PNET1–PNET6 interaction within the membrane ring, RAE1–GBPL3 interaction between the ORC and the NB, and MAD2–CRWN4 interaction between the NB and the nucleoskeleton (Fig. 4c and Extended Data Fig. 4b). In addition, three of the physical associations confirmed by the co-IP experiments (At2G27140–RAE1, HSFB2B–Nup43 and KH8–Nup43) are among the 81 high-confidence models. Collectively, these high-confidence predicted PPI models allow us to delineate an extensive PPI network beyond Nup–Nup interactions within the NPC-associated proteome (Fig. 4d), underscoring potential molecular mechanisms for the NPC to recruit diverse protein complexes through direct protein–protein interactions (Fig. 4c bottom panel).

Phase separation contributes to the assembly of the NPC proxiome

The central channel of the NPC establishes a phase-separated environment that facilitates the transport of proteins and RNA[46]. Notably, our recent findings demonstrate that GBPL3 promotes potential phase separation at the NPC basket[22], suggesting that the NPC's function may rely on phase-separated environments at multiple levels. Supporting this notion, we found that more than 70% (28/39) of known *Arabidopsis* nucleoporins contain intrinsically disordered regions (IDRs) predicted by D2P2 (Fig. 5a). Furthermore, within the NPC-associated proteome, there is a notable overrepresentation of IDR-containing proteins (IDPs)—374 out of 582 proteins (64.3%), in contrast to the genome-wide average of 29.5%. This observation hints at the possible existence of a phase-separated environment surrounding the NPC. Notably, RNA-binding proteins (RBPs), a prominent group of proteins involved in phase separation, constitute over 40% of the NPC-associated proteome (233/582) (Fig. 5b and Supplementary Table 11), which is also consistent with a major role of the NPC in mRNA metabolism.

To investigate whether phase separation plays a role in the interactions between Nups and NPC-associated IDPs, we selected two nucleoporins from the NPC cytoplasmic ring (CG1 and RAE1), two nucleoporins from the nuclear basket (Nup82 and GBPL3) and two IDR-containing RBP candidates (Extended Data Fig. 5a), including DEAD-box RNA helicase 40 (RH40, a CG1 prey) and RNA-BINDING GLYCINE-RICH PROTEIN D5 (RGBD5, a GBPL3 prey) and transiently expressed them in *Nicotiana benthamiana*. We found that when individually expressed, Nup82 and GBPL3 but not CG1 and RAE1 were able to form spontaneous nuclear condensates, as previously reported[22]. Also, RH40 but not RBGD5 frequently forms nuclear condensates that are primarily associated with the nuclear periphery (Fig. 5c). Fluorescence recovery after photobleaching (FRAP) analysis further revealed that the RH40 condensates were able to recover within a few seconds after photobleaching (Fig. 5d), suggesting active exchange of materials with their environment. In addition, we found that deletion of the N-terminal IDR domain of RH40 could substantially compromise the formation of condensates and that deleting both N- and C-terminal IDR domains in RH40 completely abolished condensate formation (Fig. 5e). These properties are consistent with biomolecular condensates whose formation is driven by liquid–liquid phase separation.

When co-expressed with RH40, CG1 and RAE1 co-localize with RH40 in nuclear condensates (Fig. 5f). However, nuclear condensates formed by Nup82 and GBPL3 do not co-localize with RH40. In contrast, RBGD5 forms nuclear condensates with GBPL3 but not with other nucleoporins. These data suggest that NPC-associated IDPs possess the ability to interact with nucleoporins through phase transition. Furthermore, this process seems to be intricately controlled, with the CG1 prey RH40 condensing exclusively with cytoplasmic nucleoporins, and the GBPL3 prey RBGD5 doing so only with the NB-localized GBPL3. We hypothesize that the composition of proteins and/or nucleic acids on each side of the NPC may significantly influence the selective phase transitions within NPC sub-environments.

Discussion

Although the NPC is known as one of the largest macromolecular assemblies within the cell, our proteomic profiling has further expanded the scope of nuclear pore-associated proteins and illuminated previously uncharted intricacies in both categories and functionalities of the NPC. Detailed analysis of the NPC-associated proteome suggests that the NPC serves as an integrated platform, orchestrating a multitude of pivotal events in gene expression, ranging from transcription and mRNA processing to mRNA export and translation regulation. This finding is in strong alignment with the gene gating mechanism previously proposed in animals and yeast research and provides a robust foundation of molecular evidence substantiating the efficient coordination of mRNA synthesis, maturation and transportation centred around the NPC. It is imperative to note, however, that our profiling use entire seedlings, and consequently, the current assembly of the NPC-associated proteome does not consider tissue- or cell-type-specific distinctions, thus not reflecting potential variations in the nuclear pore proteome.

Beyond its role in mRNA metabolism, the extended NPC proteome also offers intriguing insights into other potential functions of the NPC.

Fig. 4 | Extensive protein–protein interactions within the NPC-associated proteome. a, Co-IP of selected nucleoporins and newly identified NPC-associated proteins. Nups-GFP were transiently co-expressed with their associated preys fused to 3xHA-TurboID in *N. benthamiana*. The MATH domain-containing protein At5g26280 and BRASSINOSTEROID INSENSITIVE1 (BRI1) were used as negative controls. Protein extract was immunoprecipitated with GFP-trap beads before immunoblotting with anti-GFP and anti-HA antibodies. Co-IP experiments were repeated at least twice with similar results. **b**, Scatter plot visualizing the ipTM scores for predicted pairwise PPIs among the 109 selected nucleoporins and NPC-associated proteins using AlphaFold-Multimer and AF2Complex. These interactions were colour coded and separated into 11 groups on the basis of the functional category of one of the protein partners. High-confidence interactions are represented by triangles and square symbols above the dashed line. **c**, Top: heat maps illustrating high-confidence predicted interactions among *Arabidopsis* nucleoporins. Interactions between Nups that are supported by structural biology data from human Nups are marked with green checkmarks. Bottom: heat maps showing additional high-confidence PPIs between nucleoporins and NPC-associated proteins. **d**, The predicted PPI network within the NPC-associated proteome. Known nucleoporins are represented by rectangular nodes and newly identified NPC-associated proteins are represented by elliptical nodes.

https://doi.org/10.1038/s41477-024-01698-9

https://doi.org/10.1038/s41477-024-01698-9

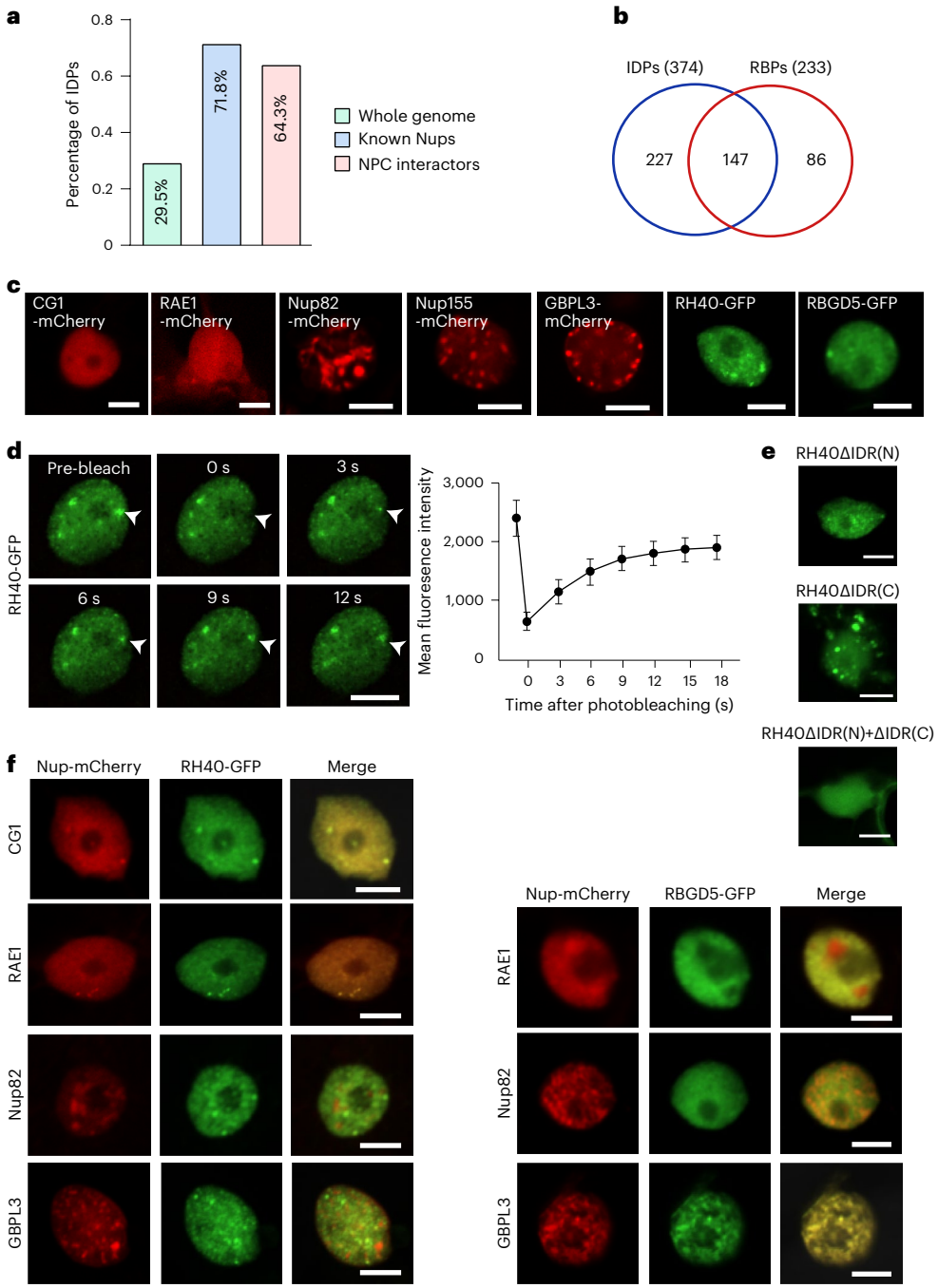

Fig. 5 | Phase separation contributes to the assembly of the nuclear pore-associated proteome. a, Bar plot illustrating the percentage of IDPs within the *Arabidopsis* whole genome, known nucleoporins and the NPC-associated proteome defined in this study. **b**, Venn diagram displaying the overlaps between IDPs and RBPs in the NPC-associated proteome. **c**, Transient protein expression of cytoplasmic filament Nup CG1 and RAE1, nuclear basket Nup Nup82 and GBPL3, and NPC-associated proteins, including the CG1 prey RH40 and the GBPL3 prey RBGD5. **d**, FRAP analysis using nuclear condensates formed by RH40. Left: nuclei, with arrowheads indicating the photobleached condensate in representative nuclei. Right: fluorescence quantification. Time 0 indicates the end of photobleaching. Data from one of the three independent experiments are shown and presented as mean ± s.d. ($n = 10$ condensates). **e**, Transient expression of RH40-GFP constructs with truncated N-terminal and/or C-terminal IDR domains. **f**, Transient co-expression of Nups-mCherry with RH40-GFP or RBGD5-GFP. The experiments in **c**–**f** were repeated independently three times with similar results. Scale bars, 10 μm.

For instance, the identification of multiple ESCRT I complex components, including ELC (VPS23a) and its homologue ELC-like (VPS23b), as shared targets of CG1 and GBPL3 (Extended Data Fig. 2a) implies a close relationship between the NPC and ESCRT. In yeast and mammalian cells, it is well-documented that the ESCRT III complex plays a pivotal role in the orchestration and reshaping of the nuclear envelope throughout the cell cycle[47,48]. While the precise mechanisms governing NE remodelling and closure at the conclusion of mitosis in plants remain unclear, it is worth noting that the plant *elc* mutant exhibits a phenotype characterized by the presence of multiple nuclei in various cell types[49], which resembles mutants in the ESCRT III complex of yeast and mammals[47,48]. In addition, we found that the plant-specific ESCRT I component, FREE1, alongside other critical ESCRT I constituents, was also specifically probed by GBPL3 and CG1. This observation sparks an intriguing idea that plant cells might have developed a distinct and exclusive mechanism for nuclear envelope remodelling and sealing.

Another example is that heat shock chaperone proteins, including members of HSP40, HSP70 and T-complex family, were probed by both FG Nups and core scaffold Nups. Supporting this observation, recent research has unveiled that chaperones form localized foci in the vicinity of the NPC and serve as pivotal factors in preventing the aggregation of FG nucleoporins. This, in turn, facilitates NPC biogenesis in humans[50,51].

On the basis of a combined biochemical and structural modelling PPI prediction analysis, we propose that direct protein interactions with nucleoporins assume a critical role in the intricate assembly of the nuclear pore-associated proteome. In parallel, we postulate that the phase separation process, mediated by IDR-containing proteins, may also contribute substantially to both the formation and maintenance of the proteome at the nuclear pore. This hypothesis is underscored by the observation that more than two-thirds of the identified NPC-associated proteins are predicted to be intrinsically disordered proteins, including many RBPs. Besides RBPs, it is well known that proteins containing FG repeats are significant contributors to phase separation within the NPC, particularly in the central channel. The phenylalanine aromatic ring within FG repeats plays a crucial role in the formation of highly elastic hydrogels and phase separation through multivalent hydrophobic interactions[6,46]. To our surprise, we found a considerable number of previously uncharacterized FG repeats-containing proteins in the NPC-associated proteome (108 in total) (Extended Data Fig. 5b and Supplementary Table 12). These proteins were defined by containing a minimum of three FG repeats within 50 amino acids or at least four FG repeats within 200 amino acids on the basis of previous investigations on animal FG repeats proteins[52,53]. This evidence suggests that FG repeats-containing proteins are highly concentrated surrounding the NPC, potentially forming an extended layer of selective cargo transport barrier outside of the NPC central channel. Indeed, a recent report on 3D tracking of cargo transport through the NPC revealed large cargo clouds near both the cytoplasmic and nucleoplasmic openings, suggesting extensive interactions of cargo/NTRs with proteins/structures far beyond the central channel of the nuclear pore[54]. Moreover, studies in *C. elegans* have shown that some FG repeats-containing RNA-binding proteins could form functional perinuclear P granules, and deletion of the FGs from these RNA-binding proteins resulted in the detachment of P granules from the nuclear membrane into the cytoplasm[55,56]. This observation is also consistent with our identification of P-body components at the cytoplasmic side of the plant NPC.

In forthcoming research, it is imperative to substantiate the recruitment of the identified NPC-associated proteins to the nuclear pore in vivo and verify the essential protein–protein interactions that underlie the assembly. Moreover, as in silico approaches develop and surpass computational limitations, more PPIs within the nuclear pore-associated proteome can be modelled and refined. Last but not least, acquiring comprehensive insights into the tissue/cell-type-specific and condition-dependent nuclear pore proteome is critical for a deeper understanding of the compositional dynamics and functional significance of the protein assembly at the nuclear pore.

Methods

Materials, plasmid construction and plant transformation

All *Arabidopsis* plants utilized in this study are Col-0 ecotype. Wild-type (WT) and transgenic *Arabidopsis* seeds were stratified at 4 °C in the dark for 2 days before being grown at 22 °C under a 16 h:8 h light:dark cycle. All constructs were generated using In-Fusion cloning (ClonExpress II One Step Cloning kit, Vazyme), unless otherwise specified. For BioID2 fusion, the full-length cDNA of *Nup50a* and gDNA of *Nup188* were cloned into a modified pEarlyGate100 vector with a *BioID2-HA* tag[29]. Similarly, for miniTurbo fusion, the full-length cDNA of *Nup54* and gDNA of *CG1* were cloned into a modified pEG100 vector with a *3xHA-miniTurbo* tag. For fluorescence protein-tagged constructs, the full-length gDNA of *EXA1*, *VPS37-1* and *VPS37B*, and the full-length cDNA of *HXK2*, *RH40*, *RGBD5* and truncated *RH40* (1–1,005 bp, 1,006–2,265 bp, 1,006–3,264 bp) were cloned into a modified pEG100 vector with a GFP tag. To generate constructs for co-IP and co-expression assays, both Gateway system and In-Fusion cloning were applied. The full-length cDNA of *Nup85*, *Nup82* and *Nup155*, and the full-length gDNA of *Nup136* were inserted into pBSDONR p1-p4, and GFP or mCherry fragment was cloned into pBSDONR p4r-p2 using BP reaction. The pBSDONR p1-p4 and pBSDONR p4r-p2 vectors were then combined and cloned into the destination vector pEG100 using LR reaction. The full-length cDNA of *RAE1*, *CG1*, *Nup43*, *Nup50b* and *Seh1* were cloned into a modified pEG100 vector with a *GFP* or *mCherry* tag. The full-length cDNA of *At2g27140*, *GRF3*, *KH8*, *HSFB2B* and *SAP18* were cloned into a modified pEG100 vector with a *3xHA-TurboID* tag. All primers used for cloning are listed in Supplementary Table 13. The *Agrobacterium*-mediated floral-dip transformation method was employed to generate transgenic plants.

Proximity labelling and proteomics analysis

The BioID2- and miniTurbo-based proximity labelling and affinity purification of biotinylated proteins have been previously described[28,29]. In brief, for each bait construct, more than 40 T_1 transgenic lines were identified via resistance selection. These lines were screened for moderate levels of bait protein expression and inducible biotinylation upon free biotin treatment using immunoblot blot with anti-HA antibody and streptavidin-HRP, respectively. It is noteworthy that none of the nucleoporin bait lines exhibited discernible distinct phenotypes compared with wild type at 1 week age, the seedling stage that we sampled. A single representative line was chosen to conduct proximity-labelling proteomics. Ten-day-old transgenic seedlings at the T_2 generation were treated with 50 µM biotin for 6 h (for miniTurbo transgenic plants) and 24 h (for BioID2 transgenic plants) at room temperature. For controls, we deliberately avoided using free biotin ligases or biotin ligases fused with free YFP. We found that these proteins usually express at high levels, leading to the induction of biotinylation in a considerably wide spectrum of proteins upon biotin treatment. This, in turn, results in highly elevated false-negative rates. Consequently, our preferred controls for ratio matrix analysis consisted of WT non-transgenic plants subjected to biotin treatment (NT, primarily to eliminate natively biotinylated proteins) and the bait transgenic plants without biotin treatment (Mock, primarily to eliminate non-specific biotinylation by the biotin ligase). Two or three biological replicates, with 0.4 g of seedlings each, were sampled. The materials were then frozen and ground into a fine powder using liquid nitrogen. Total protein extraction was performed using 2 ml of protein extraction buffer (50 mM Tris (pH 7.5), 150 mM NaCl, 0.5% Triton X-100, 0.5% Nonidet P-40, 0.5% sodium deoxycholate, plant protease inhibitor cocktail, 1 mM PMSF and 40 mM MG132). A HiTrapTM desalting column (GE Healthcare) equipped with an FPLC system was utilized to remove free biotin. The eluted protein fraction was incubated with 50 µl streptavidin-coated magnetic beads (Dynabeads MyOne Streptavidin C1, Invitrogen) for 12–16 h at 4 °C. The beads were then washed five times with protein extraction buffer and subsequently boiled with protein loading buffer containing 50 mM biotin and 1% SDS for 30 min. The total biotinylated protein was separated on SDS–PAGE gels and digested with trypsin in 50 mM ammonium bicarbonate overnight at 37 °C. The resulting peptides were collected using an aqueous solution of 1% formic acid in 50% acetonitrile and lyophilised using a Speedvac before LC–MS/MS analysis. MS/MS spectra were searched against the TAIR10 database using Proteome Discoverer (v.1.4). To select specifically enriched protein candidates, ratiometric analysis was conducted using the peptide peak areas (label free quantification, LFQ values) from the experimental and control samples and the DEP package (v.1.24.0) in R (v.4.3.2). The candidates were further filtered on the basis of the normalized peptide spectrum match (PSM) value. On the basis of nucleoporins, known interactors of each bait protein and other data quality parameters, the cut-off values for LFQ and PSM data were specified in each case. Volcano plots and

heat maps were generated in R (v.4.3.2). MS data using Nup50a, Nup54, CG1 and Nup188 as baits in this study were deposited in the PRIDE database (PXD039253), and data for PNET1, Nup82, Nup93a, KAKU4 and GBPL3 were previously published and can be found in PRIDE databases PXD015919, PXD026924 and PXD032906 refs. 22,29,33.

Immunofluorescence

Immunofluorescence imaging was performed as previously described with minor modifications[57]. Briefly, the seedlings were fixed in fixation buffer (4% paraformaldehyde, 1x PBS, 2% Triton X-100) for 4 h at room temperature. After fixation, the samples were washed three times with 1x PBS buffer and incubated with digestion buffer (1% driselase (Sigma, D8037), 0.5% cellulase (Sigma, C1794), 1% pectolyase (Sigma, P3026) in 1x PBS, 1x BSA buffer) at 37 °C for 1 h. The samples were subsequently rinsed three times with 1x PBS buffer and permeabilized in 1x PBS with 2% Triton X-100 buffer at room temperature for 2 h. The resulting samples were incubated on adhesive slides with HA tag Alexa Fluor 647 conjugated mouse antibody (ThermoFisher, 26183-A647) (1:500 dilution in 1x PBS, 1x BSA buffer) at 4 °C overnight. The slides were washed with 1x PBS buffer with 0.2% Triton X-100 at room temperature, three times for 5 min each. The slides were mounted with 20 µl of antifade mounting medium with DAPI (Beyotime, P0131) for 20 min at room temperature before imaging analysis on a Nikon N-SIM S confocal microscope.

Bioinformatics analysis

To generate the co-expression network of NPC-associated candidates with nucleoporin genes, averaged logic scores based on both microarray and RNA-seq data were retrieved from ATTED-II v.11.0 (https://atted.jp/) and visualized using a clustering heat map in R. GO enrichment analysis was performed using DAVID Bioinformatics Resources (https://david.ncifcrf.gov/). Protein–protein interactions with experimental supports were retrieved from the STRING database (https://string-db.org/) and visualized using Cytoscape (v.3.9.1). Normalized gene expression levels of *Nup82*, *Nup50a*, *KAKU4* and *GBPL3* across 79 organs and developmental stages were obtained from the high-throughput transcriptome database TraVA (Transcriptome Variation Analysis, http://travadb.org/). The prediction of IDRs in NPC-associated proteins was performed using the Database of Disordered Protein Predictions (D2P2) (https://d2p2.pro/) and the VSL2 predictor from PONDR (http://www.pondr.com/). The RNA-binding proteome in *Arabidopsis* was retrieved from a previous publication[58]. The prediction of transmembrane domains in proteins within the *Arabidopsis* genome (https://www.arabidopsis.org/) was conducted using TMHMM-2.0 (https://services.healthtech.dtu.dk/services/TMHMM-2.0/).

Prediction of protein complex structure and PPI network

Protein complexes were modelled using AlphaFold-Multimer and AF2complex (v.1.4.0), which rely on AlphaFold (v.2.3.1)[59,60]. Homologous sequences were collected from standard full databases (--db_preset=full_dbs), and all experimental protein structures, which were downloaded from the Protein Data Bank on 31 March 2023, were allowed as structural templates[61]. All heterodimer complexes with a size ≤2,500 amino acids were predicted with five multimer models (v.3) without relaxation (--models_to_relax=none)[62]. The prediction was considered reliable if the interface score from AF2complex was greater than 0.5 or the ipTM score from AlphaFold-Multimer was greater than 0.75. An additional pTM threshold of >0.3 was required to remove highly disordered proteins. The interface and iptm scores were used to construct an undirected graph using igraph (v.1.4.2) in R (v.4.1.3) to represent a putative protein–protein interaction network among the candidate NPC proteins.

Co-IP and fluorescence imaging analysis

Co-IP and fluorescence imaging analysis were performed using *Agrobacterium*-mediated transient protein expression in *N. benthamiana* as previously described[29]. For Co-IP, 0.2 g of leaves were collected and ground into fine powder in liquid nitrogen. Total protein was extracted with 1 ml of protein extraction buffer (50 mM Tris (pH 7.5), 150 mM NaCl, 0.5% Triton X-100, 0.5% Nonidet P-40, 0.5% sodium deoxycholate, protease inhibitor cocktail and 40 µm MG132). After a brief centrifugation to pellet debris, 10 µl of GFP-trap beads (ChromoTek, gtak) was added to the total protein extract, which was then incubated at 4 °C for 10 h with gentle shaking. The beads were then washed five times with protein extraction buffer, separated by SDS–PAGE and subjected to immunoblot analysis using anti-GFP (Clontech, 632381, dilution 1:5,000) and anti-HA (3F10, Roche, 11867431001, dilution 1:5,000). Fluorescence imaging and FRAP analysis were performed as previously described[63]. Briefly, FRAP data of co-expressed condensates in *N. benthamiana* leaf epidermal cells were obtained on a Nikon N-SIM S confocal microscope using the ×63 objective. Condensates were bleached using a laser intensity of 100% at 485 nm and 562 nm with 100 iterations. After photobleaching, images were continuously captured for 10 min at 5 s intervals using NIS-Elements software. Mean fluorescence intensities of the bleached region were normalized, analysis was carried out using ImageJ and the recovery curve was generated using GraphPad Prism 10.

Reporting summary

Further information on research design is available in the Nature Portfolio Reporting Summary linked to this article.

Data availability

Datasets that support the results in this study are available in the supplementary tables and source data. All the mass spectrometry proteomics data have been deposited to the ProteomeXchange Consortium via the PRIDE partner repository (Identifier: PXD039253). The high-confidence predicted heterodimer complexes are available via Zenodo at https://doi.org/10.5281/zenodo.10023066 (ref. 45). Other available databases used in this study are listed in the above 'Bioinformatics analysis'. Source data are provided with this paper.

Code availability

All scripts used in this study are available in GitHub at https://github.com/s-kyungyong/NPC_structure_prediction.

References

1. Hetzer, M. W. The nuclear envelope. *Cold Spring Harb. Perspect. Biol.* **2**, a000539 (2010).
2. Lin, D. H. & Hoelz, A. The structure of the nuclear pore complex (an update). *Annu. Rev. Biochem.* **88**, 725 (2019).
3. Strambio-De-Castillia, C., Niepel, M. & Rout, M. P. The nuclear pore complex: bridging nuclear transport and gene regulation. *Nat. Rev. Mol. Cell Biol.* **11**, 490–501 (2010).
4. Hayama, R., Rout, M. P. & Fernandez-Martinez, J. The nuclear pore complex core scaffold and permeability barrier: variations of a common theme. *Curr. Opin. Cell Biol.* **46**, 110–118 (2017).
5. Ng, S. C. et al. Barrier properties of Nup98 FG phases ruled by FG motif identity and inter-FG spacer length. *Nat. Commun.* **14**, 747 (2023).
6. Dekker, M., Van der Giessen, E. & Onck, P. R. Phase separation of intrinsically disordered FG-Nups is driven by highly dynamic FG motifs. *Proc. Natl Acad. Sci. USA* **120**, e2221804120 (2023).
7. Onischenko, E. et al. Natively unfolded FG repeats stabilize the structure of the nuclear pore complex. *Cell* **171**, 904–917.e19 (2017).
8. Hampoelz, B., Andres-Pons, A., Kastritis, P. & Beck, M. Structure and assembly of the nuclear pore complex. *Annu. Rev. Biophys.* **48**, 515–536 (2019).
9. Bley, C. J. et al. Architecture of the cytoplasmic face of the nuclear pore. *Science* **376**, eabm9129 (2022).

10. Mészáros, N. et al. Nuclear pore basket proteins are tethered to the nuclear envelope and can regulate membrane curvature. *Dev. Cell* **33**, 285–298 (2015).
11. Krull, S., Thyberg, J., Björkroth, B., Rackwitz, H. R. & Cordes, V. C. Nucleoporins as components of the nuclear pore complex core structure and Tpr as the architectural element of the nuclear basket. *Mol. Biol. Cell* **15**, 4261–4277 (2004).
12. Makarov, A. A., Padilla-Mejia, N. E. & Field, M. C. Evolution and diversification of the nuclear pore complex. *Biochem. Soc. Trans.* **49**, 1601–1619 (2021).
13. Francesca, D. N. et al. Human nucleoporins promote HIV-1 docking at the nuclear pore, nuclear import and integration. *PLoS ONE* **7**, e46037 (2012).
14. Dicks, M. D. J. et al. Multiple components of the nuclear pore complex interact with the amino-terminus of MX2 to facilitate HIV-1 restriction. *PLoS Pathog.* **14**, e1007408 (2018).
15. Sadasivan, J. et al. Targeting Nup358/RanBP2 by a viral protein disrupts stress granule formation. *PLoS Pathog.* **18**, e1010598 (2022).
16. Adams, R. L., Terry, L. J. & Wente, S. R. Nucleoporin FG domains facilitate mRNP remodeling at the cytoplasmic face of the nuclear pore complex. *Genetics* **197**, 1213–1224 (2014).
17. Gallardo, P., Salas-Pino, S. & Daga, R. R. A new role for the nuclear basket network. *Microb. Cell* **4**, 423–425 (2017).
18. Krull, S. et al. Protein Tpr is required for establishing nuclear pore-associated zones of heterochromatin exclusion. *EMBO J.* **29**, 1659–1673 (2010).
19. Taddei, A. et al. Nuclear pore association confers optimal expression levels for an inducible yeast gene. *Nature* **441**, 774–778 (2006).
20. Cibulka, J., Bisaccia, F., Radisavljević, K., Gudino Carrillo, R. M. & Köhler, A. Assembly principle of a membrane-anchored nuclear pore basket scaffold. *Sci. Adv.* **8**, eabl6863 (2022).
21. Tamura, K., Fukao, Y., Hatsugai, N., Katagiri, F. & Hara-Nishimura, I. Nup82 functions redundantly with Nup136 in a salicylic acid-dependent defense response of *Arabidopsis thaliana*. *Nucleus* **8**, 301–311 (2017).
22. Tang, Y., Ho, M. I., Kang, B.-H. & Gu, Y. GBPL3 localizes to the nuclear pore complex and functionally connects the nuclear basket with the nucleoskeleton in plants. *PLoS Biol.* **20**, e3001831 (2022).
23. Schuller, A. P. et al. The cellular environment shapes the nuclear pore complex architecture. *Nature* **598**, 667–671 (2021).
24. Akey, C. W. et al. Comprehensive structure and functional adaptations of the yeast nuclear pore complex. *Cell* **185**, 361–378. e25 (2022).
25. Zimmerli, C. E. et al. Nuclear pores dilate and constrict in cellulo. *Science* **374**, eabd9776 (2021).
26. Lusk, C. P. & King, M. C. Nuclear pore complexes feel the strain. *Mol. Cell* **81**, 4962–4963 (2021).
27. Vial, A. et al. Structure and mechanics of the human nuclear pore complex basket using correlative AFM-fluorescence superresolution microscopy. *Nanoscale* **15**, 5756–5770 (2023).
28. Huang, A. et al. Proximity labeling proteomics reveals critical regulators for inner nuclear membrane protein degradation in plants. *Nat. Commun.* **11**, 3284 (2020).
29. Tang, Y., Huang, A. & Gu, Y. Global profiling of plant nuclear membrane proteome in *Arabidopsis*. *Nat. Plants* **6**, 838–847 (2020).
30. Holzer, G. et al. The nucleoporin Nup50 activates the Ran guanine nucleotide exchange factor RCC1 to promote NPC assembly at the end of mitosis. *EMBO J.* **40**, e108788 (2021).
31. Tamura, K., Fukao, Y., Iwamoto, M., Haraguchi, T. & Hara-Nishimura, I. Identification and characterization of nuclear pore complex components in *Arabidopsis thaliana*. *Plant Cell* **22**, 4084–4097 (2010).
32. Sun, C., Fu, G., Ciziene, D., Stewart, M. & Musser, S. M. Choreography of importin-α/CAS complex assembly and disassembly at nuclear pores. *Proc. Natl Acad. Sci. USA* **110**, E1584–E1593 (2013).
33. Tang, Y., Dong, Q., Wang, T., Gong, L. & Gu, Y. PNET2 is a component of the plant nuclear lamina and is required for proper genome organization and activity. *Dev. Cell* **57**, 19–31.e6 (2022).
34. Jia, M., Chen, X., Shi, X., Fang, Y. & Gu, Y. Nuclear transport receptor KA120 regulates molecular condensation of MAC3 to coordinate plant immune activation. *Cell Host Microbe* **31**, 1685–1699.e7 (2023).
35. Maldonado-Bonilla, L. D. Composition and function of P bodies in *Arabidopsis thaliana*. *Front. Plant Sci.* **5**, 201 (2014).
36. Huh, S. U. The role of Pumilio RNA binding protein in plants. *Biomolecules* **11**, 1851 (2021).
37. Jiménez-López, D., Bravo, J. & Guzmán, P. Evolutionary history exposes radical diversification among classes of interaction partners of the MLLE domain of plant poly (A)-binding proteins. *BMC Evol. Biol.* **15**, 195 (2015).
38. Arribas-Hernández, L. et al. Recurrent requirement for the m6A-ECT2/ECT3/ECT4 axis in the control of cell proliferation during plant organogenesis. *Development* **147**, dev189134 (2020).
39. Arae, T. et al. Identification of *Arabidopsis* CCR4-NOT complexes with pumilio RNA-binding proteins, APUM5 and APUM2. *Plant Cell Physiol.* **60**, 2015–2025 (2019).
40. Sheth, U., Pitt, J., Dennis, S. & Priess, J. R. Perinuclear P granules are the principal sites of mRNA export in adult *C. elegans* germ cells. *Development* **137**, 1305–1314 (2010).
41. Holla, S. et al. Positioning heterochromatin at the nuclear periphery suppresses histone turnover to promote epigenetic inheritance. *Cell* **180**, 150–164. e15 (2020).
42. Lautier, O. et al. Co-translational assembly and localized translation of nucleoporins in nuclear pore complex biogenesis. *Mol. Cell* **81**, 2417–2427.e5 (2021).
43. Morrison, D. K. The 14-3-3 proteins: integrators of diverse signaling cues that impact cell fate and cancer development. *Trends Cell Biol.* **19**, 16–23 (2009).
44. de Boer, A. H., van Kleeff, P. J. & Gao, J. Plant 14-3-3 proteins as spiders in a web of phosphorylation. *Protoplasma* **250**, 425–440 (2013).
45. Tang, Y. et al. Proximity labeling-based profiling reveals a central role of the nuclear pore in mRNA metabolism. *Zenodo* https://doi.org/10.5281/zenodo.10023066 (2023).
46. Nag, N., Sasidharan, S., Uversky, V. N., Saudagar, P. & Tripathi, T. Phase separation of FG-nucleoporins in nuclear pore complexes. *Biochim. Biophys. Acta* **1869**, 119205 (2022).
47. Tang, Y. Plant nuclear envelope as a hub connecting genome organization with regulation of gene expression. *Nucleus* **14**, 2178201 (2023).
48. Webster, B. M. et al. Chm7 and Heh1 collaborate to link nuclear pore complex quality control with nuclear envelope sealing. *EMBO J.* **35**, 2447–2467 (2016).
49. Spitzer, C. et al. The *Arabidopsis* elch mutant reveals functions of an ESCRT component in cytokinesis. *Development* **133**, 4679–4689 (2006).
50. Prophet, S. M. et al. Atypical nuclear envelope condensates linked to neurological disorders reveal nucleoporin-directed chaperone activities. *Nat. Cell Biol.* **24**, 1630–1641 (2022).
51. Kuiper, E. F. E. et al. The chaperone DNAJB6 surveils FG-nucleoporins and is required for interphase nuclear pore complex biogenesis. *Nat. Cell Biol.* **24**, 1584–1594 (2022).
52. Frey, S. & Gorlich, D. A saturated FG-repeat hydrogel can reproduce the permeability properties of nuclear pore complexes. *Cell* **130**, 512–523 (2007).

53. Shinkai, Y., Kuramochi, M. & Miyafusa, T. New family members of FG repeat proteins and their unexplored roles during phase separation. *Front. Cell Dev. Biol.* **9**, 708702 (2021).
54. Chowdhury, R., Sau, A. & Musser, S. M. Super-resolved 3D tracking of cargo transport through nuclear pore complexes. *Nat. Cell Biol.* **24**, 112–122 (2022).
55. Updike, D. L., Hachey, S. J., Kreher, J. & Strome, S. P granules extend the nuclear pore complex environment in the *C. elegans* germ line. *J. Cell Biol.* **192**, 939–948 (2011).
56. Voronina, E. & Seydoux, G. The *C. elegans* homolog of nucleoporin Nup98 is required for the integrity and function of germline P granules. *Development* **137**, 1441–1450 (2010).
57. Wang, N. et al. The plant nuclear lamina disassembles to regulate genome folding in stress conditions. *Nat. Plants* **9**, 1081–1093 (2023).
58. Marondedze, C. The increasing diversity and complexity of the RNA-binding protein repertoire in plants. *Proc. R. Soc. B* **287**, 20201397 (2020).
59. Gao, M., Nakajima An, D., Parks, J. M. & Skolnick, J. AF2Complex predicts direct physical interactions in multimeric proteins with deep learning. *Nat. Commun.* **13**, 1744 (2022).
60. Jumper, J. et al. Highly accurate protein structure prediction with AlphaFold. *Nature* **596**, 583–589 (2021).
61. Berman, H. M. et al. The Protein Data Bank. *Nucleic Acids Res.* **28**, 235–242 (2000).
62. Evans, R. et al. Protein complex prediction with AlphaFold-Multimer. Preprint at *bioRxiv* https://doi.org/10.1101/2021.10.04.463034 (2022).
63. Zhou, X., Tamura, K., Graumann, K. & Meier, I. Exploring the protein composition of the plant nuclear envelope. *Methods Mol. Biol.* **1411**, 45–65 (2016).

Acknowledgements

This work was supported by the Young Taishan Scholars Program of Shandong Province (to Y.T.), the National Institutes of Health Director's Award (1DP2AT011967-01, to K.K.), and funds from the US National Science Foundation (MCB 2049931, to Y.G.) and the USDA National Institute of Food and Agriculture (HATCH project CA-B-PLB-0243-H, to Y.G.).

Author contributions

Y.T., Q.Z. and Y.G. designed the research. Y.T., A.H. and M.L. performed proximity-labelling proteomics experiments. K.S. and K.K. performed protein–protein interaction prediction using AlphaFold-Multimer and AF2Complex. Y.T., X.Y. and M.Y. performed protein localization and co-IP analysis. Y.T. performed all other experiments. Y.T. and Y.G. wrote the paper. All authors analysed the data, discussed the results and edited the manuscript.

Competing interests

The authors declare no competing interests.

Additional information

Extended data is available for this paper at https://doi.org/10.1038/s41477-024-01698-9.

Supplementary information The online version contains supplementary material available at https://doi.org/10.1038/s41477-024-01698-9.

Correspondence and requests for materials should be addressed to Yangnan Gu.

Peer review information *Nature Plants* thanks Sachihiro Matsunaga and the other, anonymous, reviewer(s) for their contribution to the peer review of this work.

https://doi.org/10.1038/s41477-024-01698-9

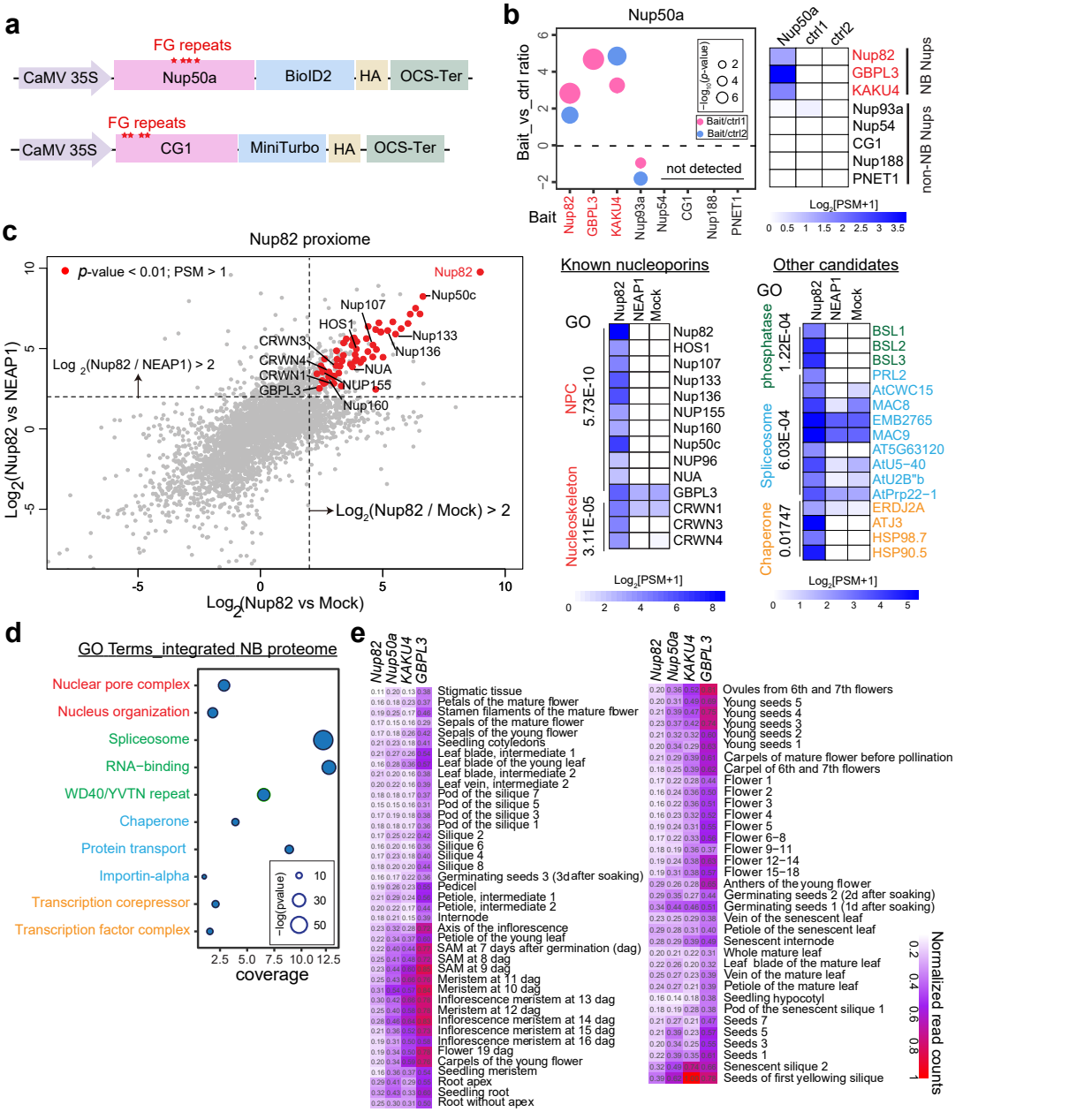

Extended Data Fig. 1 | Nuclear basket proxiome reveals robust association of NPC with the spliceosome. a, Schematic diagrams illustrating the DNA constructs carried by transgenic *Arabidopsis* plants utilized for proximity labeling (PL) proteomics. The positions of FG repeats are marked with red stars on Nup50a and CG1. **b**, Bubble plot presenting the reanalysis of PL proteomic data obtained using different Nups as bait. The left side displays LFQ intensity values of Nup50a protein, while the right side features a heatmap showing normalized peptide spectrum match (PSM) values of Nup50a. Controls for Nup82 and Nup93a are biotin-treated NEAP1-BioID2 sample (Ctrl 1) and mock-treated YFP-BioID2 sample (Ctrl 2). For GBPL3, non-transformant plants (NT) served as control (Ctrl 1). Controls for KAKU4, Nup188, and PNET1 were NT plants (Ctrl 1) and mock-treated YFP-BioID2 samples (Ctrl 2). For CG1 and Nup54, NT plants (Ctrl 1) and mock-treated transgenic plants (Ctrl 2) were used as controls. **c**, Scatter plot showing candidates identified in the Nup82 proxiome. Known nucleoporins and nucleoskeleton proteins are labeled. Controls for ratiometric analysis included NEAP1-BioID2 and mock samples. Three biological replicates were utilized for each sample. Significantly enriched protein candidates, denoted by red dots, were selected using cutoffs p-value < 0.01, fold-change > 4, and PSM > 1. On the right, GO enrichment analysis and heatmaps displaying averaged PSM values of known nucleoporins and other candidates in the Nup82 proxiome are presented. **d**, GO enrichment analysis of the integrated nuclear basket proxiome consisting of 423 proteins. Representative GO terms are displayed. **e**, Gene expression patterns of *Nup82*, *Nup50a*, *KAKU4*, and *GBPL3* in different tissues and developmental stages of Arabidopsis. Transcriptomic data were retrieved from the TraVA database (Transcriptome Variation Analysis, http://travadb.org/). For protein candidates identified by proximity labeling, statistical tests were two-sided t-tests without adjustment (**b** and **c**). Statistical tests used for GO analysis in (**c** and **d**) were one-sided Fisher's Exact tests with multiple comparison adjustments.

https://doi.org/10.1038/s41477-024-01698-9

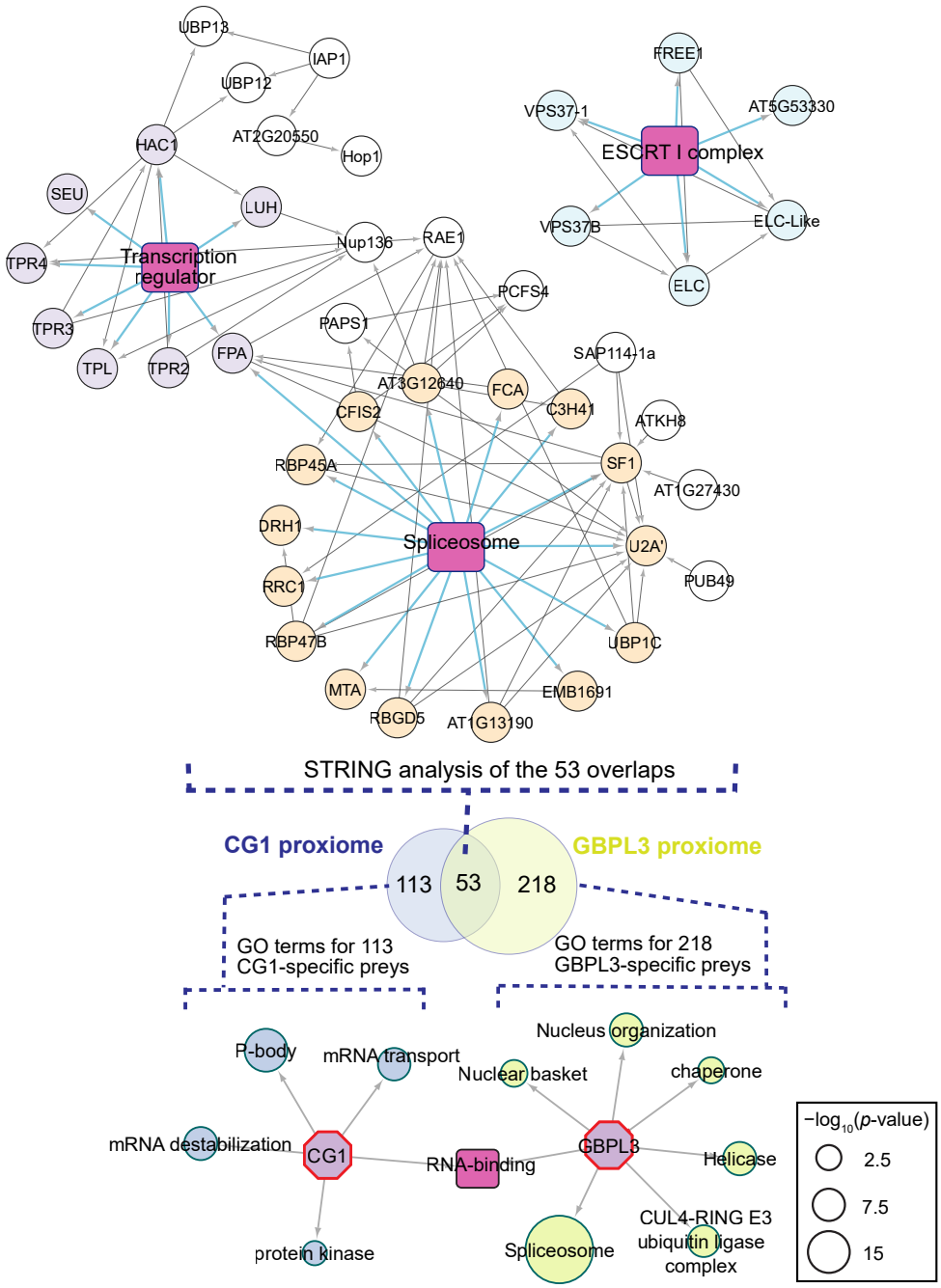

Extended Data Fig. 2 | Comparative analysis of the CG1 proxiome and the GBPL3 proxiome. The middle Venn diagram illustrates the overlaps and specific proteins probed by CG1 and GBPL3 using proximity labeling proteomics. The upper panel presents a combined GO analysis (red squares and blue edges) and protein-protein interaction analysis (gray edges, STRING) using the 53 overlapping preys probed by both CG1 and GBPL3. The lower panel displays GO analyses, and the GO terms of CG1 and GBPL3 specific preys are labeled with blue and yellow circles, respectively. The common GO term 'RNA binding' is positioned in the middle and labeled with a red square. Statistical tests used for GO analysis were one-sided Fisher's Exact tests with multiple comparison adjustments.

https://doi.org/10.1038/s41477-024-01698-9

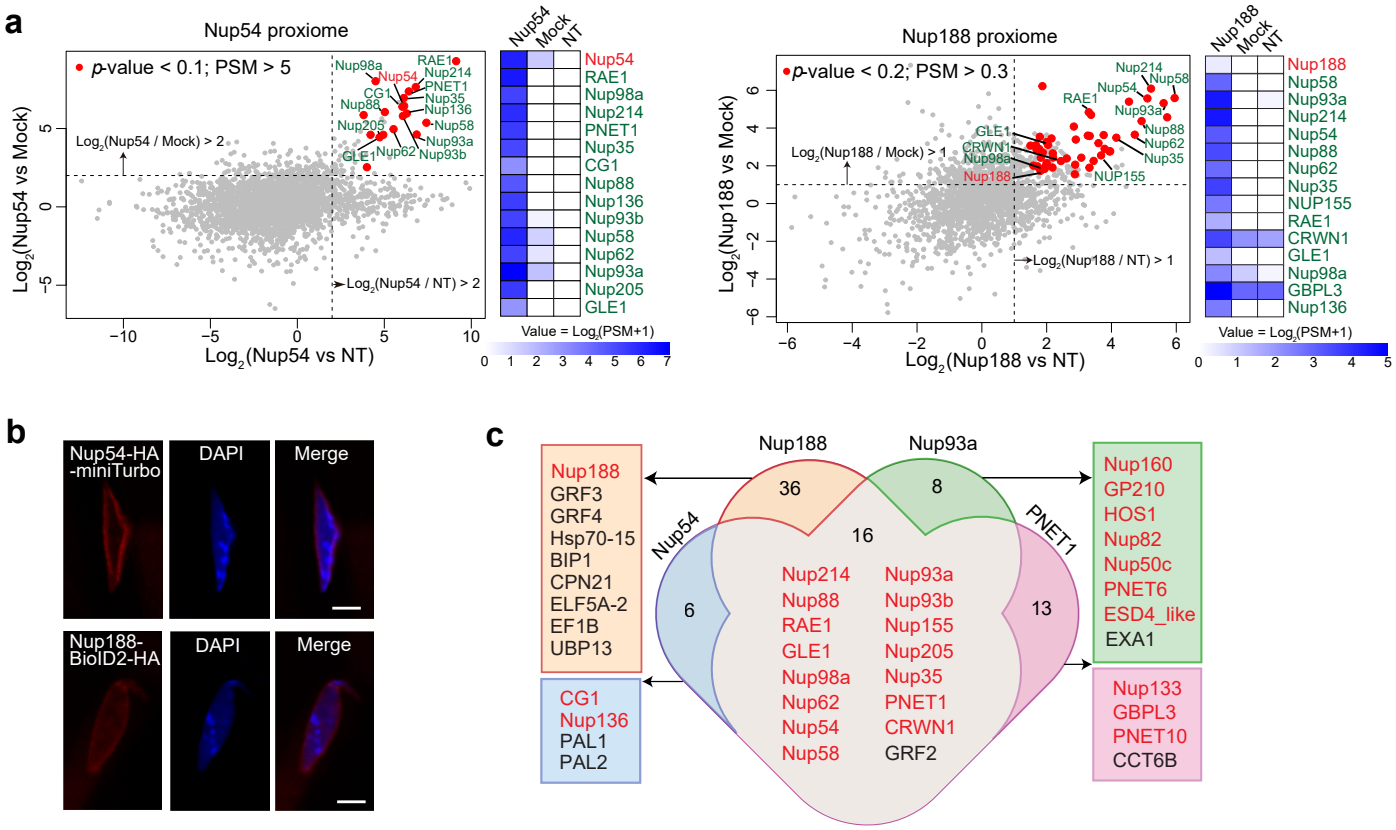

Extended Data Fig. 3 | Assembly of the NPC core scaffold proxiome. a, Scatter plots displaying candidates identified in the Nup54 and Nup188 proxiomes. Mock-treated and non-transformant (NT) samples were used as controls for ratiometric analysis. Two biological replicates were used for the Nup54 proxiome, while three replicates were used for the Nup188 proxiome. Significantly enriched protein candidates were selected based on the following cutoffs: p-value < 0.1, fold-change > 2, and PSM > 5 for Nup54 proxiome; and p-value < 0.2, fold-change > 2, and PSM > 0.3 for Nup188 proxiome. Enriched candidates are represented by red dots and labeled in green text. Heatmaps illustrate the normalized average PSM values of the known nucleoporins. Statistical analyses were two-sided t-tests without adjustment. Underlying data can be found in Supplementary Table 5 and 6. **b**, Representative confocal images of the protein localization of Nup54-3xHA-miniTurbo and Nup188-BioID2-HA in transgenic plants by immunostaining using HA antibody. DAPI was used to stain the nucleus. The localization patterns have been repeated in three independent experiments with similar results. Bars = 10 µm. **c**, Assembly of the NPC core scaffold proxiome. Venn diagram representing the assembled NPC core scaffold proxiome probed by nucleoporins located at or near the NPC core. Known NPC and NE proteins are highlighted in red.

https://doi.org/10.1038/s41477-024-01698-9

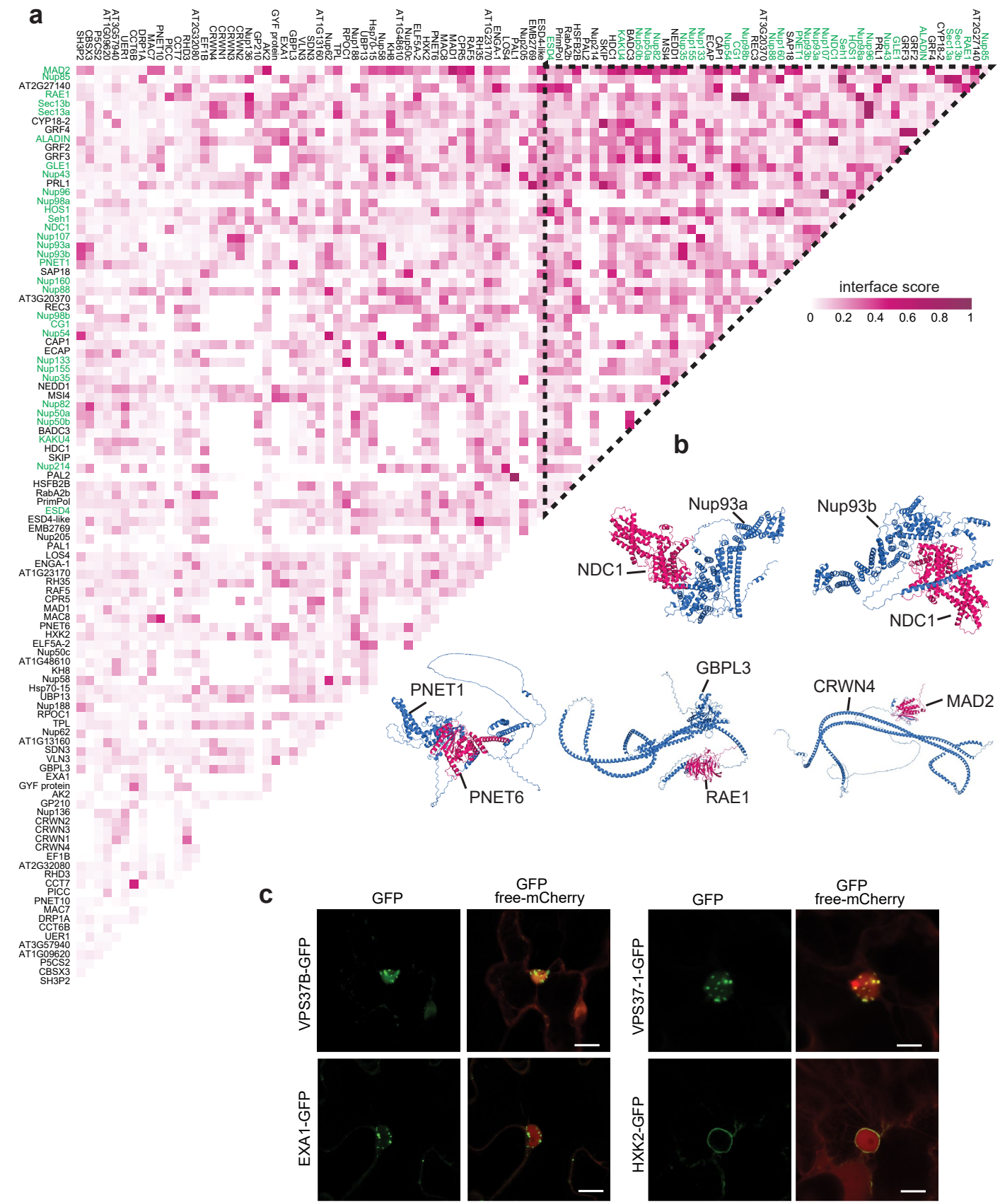

Extended Data Fig. 4 | See next page for caption.

https://doi.org/10.1038/s41477-024-01698-9

Extended Data Fig. 4 | Predicted protein-protein interactions within the extended NPC proteome. a, Pairwise interaction matrix of the 109 selected proteins within the NPC-associated proteome. The predicted interactions were generated using Alphafold-Multimer, and the interface scores derived from AF2Complex were plotted. The subgroup of proteins with strong interactions, located in the upper right corner of the matrix, is highlighted with dashed lines and green text label. **b**, Structure models depicting the predicted interactions between the following protein pairs: Nup93a and NDC1, Nup93b and NDC1, PNET1 and PNET6, GBPL3 and RAE1, and CRWN4 and MAD2. **c**, Nuclear membrane localization of selected candidates in NPC-associated proteome. GFP fusion constructs were transiently coexpressed with free mCherry in *N. benthamiana*. The localization patterns have been repeated in three independent experiments with similar results. Bars = 10 μm.

https://doi.org/10.1038/s41477-024-01698-9

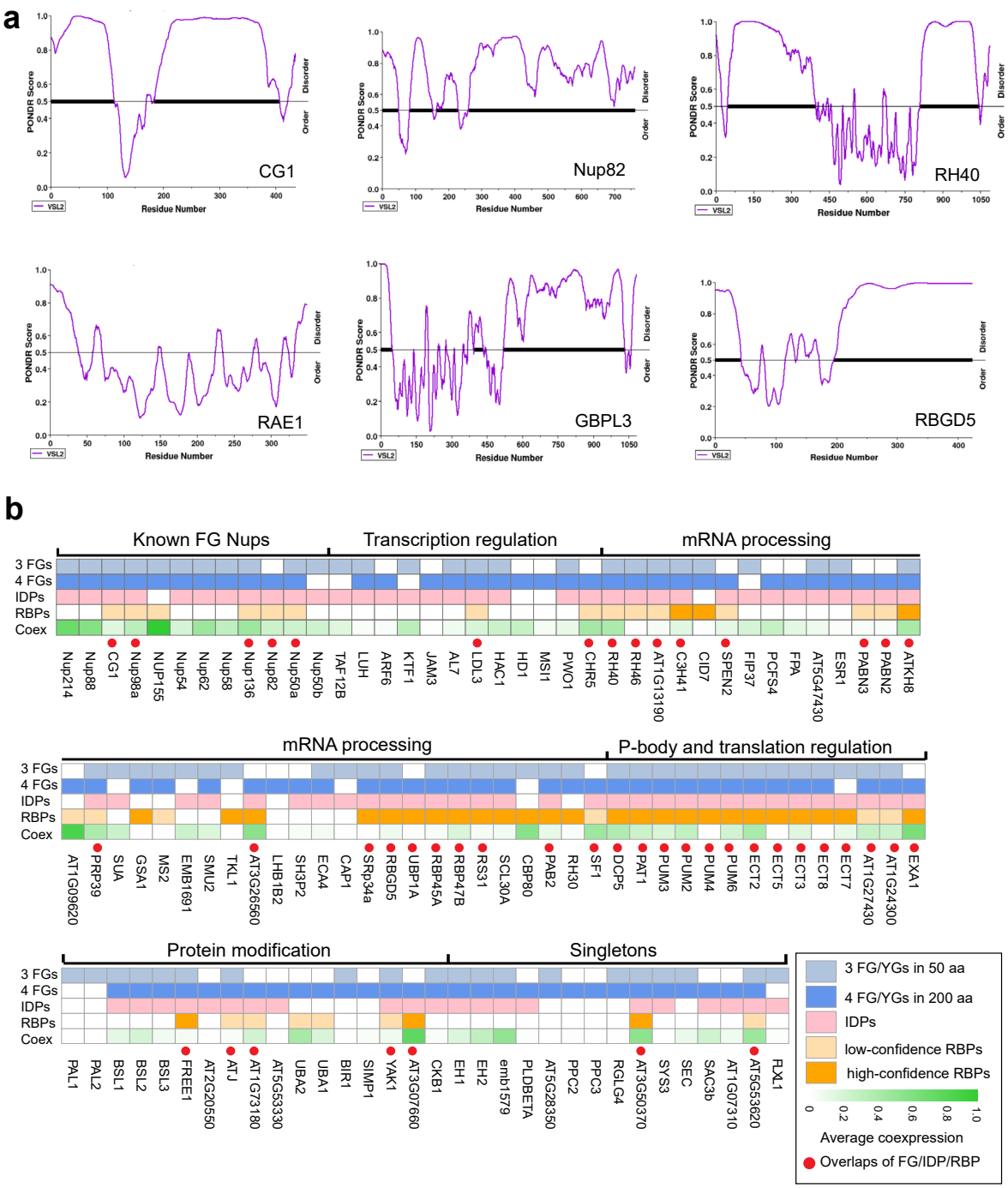

Extended Data Fig. 5 | Nucleoporins and NPC-associated proteins are enriched in intrinsically disordered regions and FG-repeats. a, Intrinsically disordered domains in selected Nups and NPC-associated proteins predicted by PONDR. **b**, Summary of NPC-associated FG repeats-containing proteins. Based on known Arabidopsis FG nucleoporins and previous investigations on FG repeats-containing proteins in animals, we used four criteria to determine FG repeats-containing proteins in Arabidopsis. Firstly, a functionally relevant FG repeat domain should contain a minimum of three FG repeats within 50 amino acids or at least four FG repeats within 200 amino acids. Secondly, Tyrosine-Glycine (YG) repeats are considered to function similar to FG repeats. Thirdly, we excluded candidates that possessed FG dipeptides within predicted transmembrane domains. Lastly, FG repeats were required to localize within predicted IDRs of a protein. By applying these criteria, we identified a total of 108 FG repeats-containing proteins in the NPC-associated proteome. D2P2 database and RNA-binding protein repertoire were used to determine whether they are also intrinsically disordered proteins (IDPs) and RNA-binding proteins (RBPs). RBPs were further divided into RBPs with high and low confidence, which were colored with light orange and dark orange, respectively. The bottom heatmap displays their average coexpression values with all known nucleoporins.

nature portfolio

Corresponding author(s): Yangnan Gu

Last updated by author(s): Mar 25, 2024

Reporting Summary

Nature Portfolio wishes to improve the reproducibility of the work that we publish. This form provides structure for consistency and transparency in reporting. For further information on Nature Portfolio policies, see our Editorial Policies and the Editorial Policy Checklist.

Statistics

For all statistical analyses, confirm that the following items are present in the figure legend, table legend, main text, or Methods section.

n/a	Confirmed	
☐	☒	The exact sample size (*n*) for each experimental group/condition, given as a discrete number and unit of measurement
☐	☒	A statement on whether measurements were taken from distinct samples or whether the same sample was measured repeatedly
☐	☒	The statistical test(s) used AND whether they are one- or two-sided *Only common tests should be described solely by name; describe more complex techniques in the Methods section.*
☒	☐	A description of all covariates tested
☐	☒	A description of any assumptions or corrections, such as tests of normality and adjustment for multiple comparisons
☐	☒	A full description of the statistical parameters including central tendency (e.g. means) or other basic estimates (e.g. regression coefficient) AND variation (e.g. standard deviation) or associated estimates of uncertainty (e.g. confidence intervals)
☐	☒	For null hypothesis testing, the test statistic (e.g. *F*, *t*, *r*) with confidence intervals, effect sizes, degrees of freedom and *P* value noted *Give P values as exact values whenever suitable.*
☒	☐	For Bayesian analysis, information on the choice of priors and Markov chain Monte Carlo settings
☒	☐	For hierarchical and complex designs, identification of the appropriate level for tests and full reporting of outcomes
☒	☐	Estimates of effect sizes (e.g. Cohen's *d*, Pearson's *r*), indicating how they were calculated

Our web collection on statistics for biologists contains articles on many of the points above.

Software and code

Policy information about availability of computer code

Data collection	Peptide identification was conducted using software Proteome Discoverer (version 1.4) developed by Thermo Scientific in LCMS workflow. Protein complexes were modeled using AlphaFold-Multimer and AF2complex (version 1.4.0), which relies on Alphafold (version 2.3.1).
Data analysis	R (version 4.3.2 and version 4.1.3) GraphPad Prism (version 10) Cytoscape (version 3.9.1) igraph (version 1.4.2) DEP package (version 1.24.0) The scripts for in silico prediction of protein-protein interaction are available in github (https://github.com/s-kyungyong/NPC_structure_prediction).

For manuscripts utilizing custom algorithms or software that are central to the research but not yet described in published literature, software must be made available to editors and reviewers. We strongly encourage code deposition in a community repository (e.g. GitHub). See the Nature Portfolio guidelines for submitting code & software for further information.

Data

Policy information about availability of data

All manuscripts must include a data availability statement. This statement should provide the following information, where applicable:

- Accession codes, unique identifiers, or web links for publicly available datasets
- A description of any restrictions on data availability
- For clinical datasets or third party data, please ensure that the statement adheres to our policy

All data used in this study are publicly available from the database or repository as described below.
Microarray and RNA-seq data were downloaded from ATTED-II (https://atted.jp/).
Gene Ontology analysis was performed using online tool DAVID Bioinformatics Resources (https://david.ncifcrf.gov/).
Protein-protein interaction data supported by experiments were downloaded from the STRING database (https://string-db.org/).
Gene expression levels were retrieved from the TraVA database (Transcriptome Variation Analysis, http://travadb.org/).
Prediction of intrinsically disordered regions (IDRs) was performed using D2P2 database (https://d2p2.pro/) and PONDR (http://www.pondr.com/).
Prediction of transmembrane domain was performed using online tool TMHMM - 2.0 (https://services.healthtech.dtu.dk/services/TMHMM-2.0/).
All the mass spectrometry proteomic data are publicly available at the PRIDE database under the accession numbers PXD039253, PXD015919, PXD026924, and PXD032906.
High-confidence predicted heterodimer complexes are available in the Zenodo repository, which are accessible with the following links: https://zenodo.org/records/10023066 or https://doi.org/10.5281/zenodo.10023066.

Research involving human participants, their data, or biological material

Policy information about studies with human participants or human data. See also policy information about sex, gender (identity/presentation), and sexual orientation and race, ethnicity and racism.

Reporting on sex and gender	not applicable
Reporting on race, ethnicity, or other socially relevant groupings	not applicable
Population characteristics	not applicable
Recruitment	not applicable
Ethics oversight	not applicable

Note that full information on the approval of the study protocol must also be provided in the manuscript.

Field-specific reporting

Please select the one below that is the best fit for your research. If you are not sure, read the appropriate sections before making your selection.

☒ Life sciences ☐ Behavioural & social sciences ☐ Ecological, evolutionary & environmental sciences

For a reference copy of the document with all sections, see nature.com/documents/nr-reporting-summary-flat.pdf

Life sciences study design

All studies must disclose on these points even when the disclosure is negative.

Sample size	No statistical approach was employed to predetermine the sample size; instead, sample sizes were based on prior experimental experience with similar assays. For mass spectrometry experiments performed in this study, the weight of each batch of harvested plant material was approximately 0.45 g, consisting of about 100 seedlings of 7-day old.
Data exclusions	No data were excluded from the analyses.
Replication	Each type of mass spectrometry sample (genotype-treatment combination) comprises two or three biological replicates, which is standard in mass spectrometry research. These independent replicates of each sample type displayed high levels of consistency based on principal component analysis of the MS results. Data analyses were conducted using all replicate samples to derive statistical inferences for candidate protein selection. Immunoblot and fluorescent imaging data underwent independent replication for two or three times, ensuring the generation of consistent and representative results.
Randomization	All plant seedlings were randomly included into biological replicates for MS experiments. In proximity-labeling proteomic experiments, samples were collected based on genotypes and treatments. Approximate 100 Arabidopsis seedlings of a specific genotype were randomly selected for treatments (+/- 50 uM biotin) and pooled as a MS sample. Similarly, N. benthamiana leaves expressing target proteins were randomly chosen for immunoblot and fluorescent imaging analyses.

Blinding	Blinding was not applicable as all experiments were performed with no prior expected results, and this study was independent of observer bias.

Reporting for specific materials, systems and methods

We require information from authors about some types of materials, experimental systems and methods used in many studies. Here, indicate whether each material, system or method listed is relevant to your study. If you are not sure if a list item applies to your research, read the appropriate section before selecting a response.

Materials & experimental systems

n/a	Involved in the study
☐	☒ Antibodies
☒	☐ Eukaryotic cell lines
☒	☐ Palaeontology and archaeology
☒	☐ Animals and other organisms
☒	☐ Clinical data
☒	☐ Dual use research of concern
☐	☒ Plants

Methods

n/a	Involved in the study
☒	☐ ChIP-seq
☒	☐ Flow cytometry
☒	☐ MRI-based neuroimaging

Antibodies

Antibodies used	anti-HA(3F10,Roche, Cat#11867431001), anti-GFP(JL-8, Clontech, Cat #632381), HA tag Alexa Fluor 647 conjugated mouse antibody (2-2.2.14, ThermoFisher, Cat#26183-A647)
Validation	All antibodies have been validated by the vendors and ourselves. Anti-HA (3F10 is a monoclonal antibody to the HA-peptide (YPYDVPDYA), derived from the influenza hemagglutinin protein, raised in a rat. It is suitable for the immunochemical detection of native influenza hemagglutinin protein and recombinant proteins that contain the HA epitope in dot blots, ELISA, western blots, immuno-cytochemistry, and immunoprecipitation.) We used 1: 5000 dilution for western blot. Additional information from the manufactures: https://www.sigmaaldrich.cn/CN/en/product/roche/roahaha. Anti-GFP (JL-8 is a monoclonal antibody to the full-length Aequorea victoria green fluorescent protein (GFP) produced by hybridoma cells, raised in a rabbit. It recognizes native and denatured forms of EGFP, EYFP, ECFP variants, and both N- and C-terminal fusion proteins containing these GFP variants. It is used for the western blot and immunoprecipitation.) We used 1:5000 dilution for western blot. Additional information from the manufactures: https://www.takarabio.com/products/antibodies-and-elisa/fluorescent-protein-antibodies/green-fluorescent-protein-antibodies?catalog=632475. HA tag Alexa Fluor 647 conjugated mouse antibody (2-2.2.14 is a mouse monocolonal antibody conjugated to Alexa Fluor® 647 fluorescent dye and tested in-house for direct flow cytometry and immunofluorescent analysis in cells expressed with HA-tagged protein. We used 1:500 dilution in 1xPBS for immunofluorescence. Additional information from the manufactures: https://www.thermofisher.com/antibody/product/HA-Tag-Antibody-clone-2-2-2-14-Monoclonal/26183-A647.

Plants

Seed stocks	All Arabidopsis plants are Col-0 ecotype, including wild type (WT) and four transgenic plants expressing Nup50a-BioID2, CG1-MiniTurbo, Nup54-MiniTurbo, and Nup188-BioID2.
Novel plant genotypes	All Arabidopsis transgenic plants were generated using Agrobacterium-mediated floral-dip transformation method. For proximity-labeling proteomic experiments, at least 20 T1 independent transgenic lines were subjected to immunoblot analysis to select an optimal line for proximity-labeling proteomic experiments. Seedlings of T2 generation were used for MS analysis.
Authentication	Authentication was not applicable.